Two-dimentional oxide quasicrystal approximants with tunable electronic and magnetic properties

Supporting information

Thiago T. Dorini[a,b], Florian Brix[a,b], Corentin Chatelier[a,b], Anton Kokalj[b,c], Émilie Gaudry*[a,b]

Structure of the OQA/Me

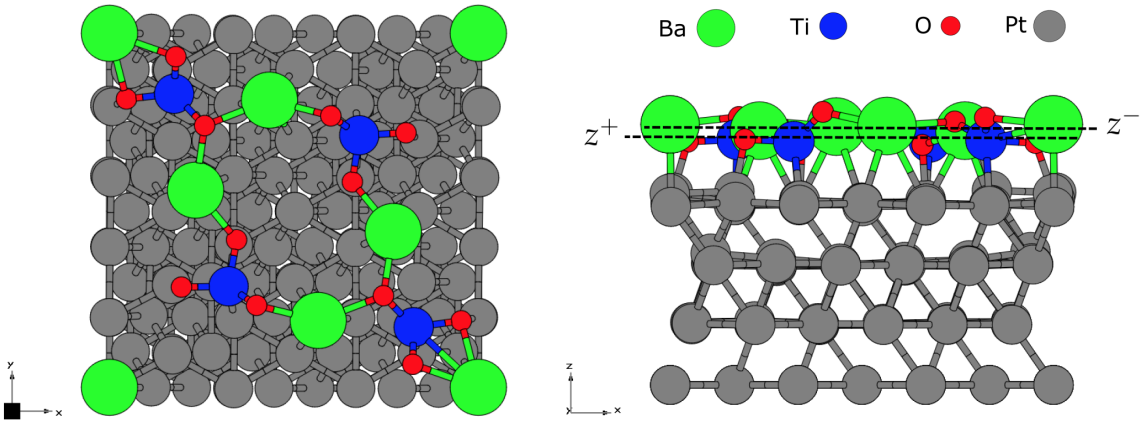

Figure S1: Top and side views of the relaxed $BaTiO_3$/Pt(111) structure.

[a] *Université de Lorraine, CNRS, Institut Jean Lamour – UMR 7198, F-54011, Nancy, France. E-mail: Emilie.Gaudry@univ-lorraine.fr*
[b] *International Associated Laboratory PACS2, CNRS Université de Lorraine, Nancy, France*
[c] *Jožef Stefan Institute, Jamova cesta 39, 1000 Ljubljana, Slovenia*
[a] *Université de Lorraine, CNRS, Institut Jean Lamour – UMR 7198, F-54011, Nancy, France. E-mail: Emilie.Gaudry@univ-lorraine.fr*
[b] *International Associated Laboratory PACS2, CNRS Université de Lorraine, Nancy, France*
[c] *Jožef Stefan Institute, Jamova cesta 39, 1000 Ljubljana, Slovenia*

Formation enthalpies

Freestanding layers

Reaction 0 ($r0$): Oxide Quasicrystal Approximant (OQA): 5/2 Ba + $4B$ + $6O_2$ → $Ba_5B_4O_{12}$

Reaction 0' ($r'0$): Single-layer Oxide Honeycomb Structure (SHS) : Ba + $4B$ + $3O_2$ → BaB_4O_6

Table S1: Formation enthalpies ($T = 0$ K) of the freestanding layers.

	$BaTiO_3$	$SrTiO_3$	$BaFeO_3$	$BaCoO_3$	$BaNiO_3$
			OQA		
ΔH_f (eV/at.)	−2.02	−2.04	−1.14	−1.12	−0.84
			SHS		
ΔH_f (eV/at.)	−1.05	−1.20	0.00	−0.40	0.38

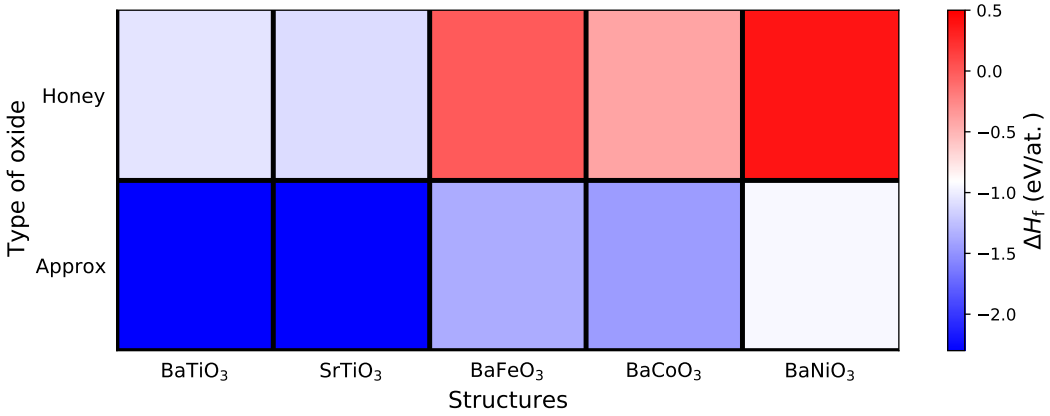

Figure S2: Formation enthalpies ($T = 0$ K), according to r0 and r'0.

Supported layers

Reaction 1 (r1): Oxide Quasicrystal Approximant (OQA): $5\mathrm{Ba} + 4B + 6\mathrm{O_2} + \mathrm{Pt_{120}} \rightarrow \mathrm{Pt_{120}Ba_5}B_4\mathrm{O_{12}}$

Reaction 2 (r2): Thick Perovskite Film (TPF) : $8\mathrm{Ba} + 6B + 6\mathrm{O_2} + \mathrm{Pt_{32}} \rightarrow \mathrm{Pt_{32}Ba_8}B_6\mathrm{O_{24}}$

Reaction 3 (r3): Single-layer Oxide Honeycomb Structure (SHS) : $\mathrm{Ba} + 4B + 3\mathrm{O_2} + \mathrm{Pt_{32}} \rightarrow \mathrm{Pt_{32}Ba}B_4\mathrm{O_6}$

Table S2: Formation enthalpy of the supported OQA ($T = 0$ K), according to $5\mathrm{Ba} + 4B + 6\mathrm{O_2} + \mathrm{Pt_{120}} \rightarrow \mathrm{Pt_{120}Ba_5}B_4\mathrm{O_{12}}$

	$BaTiO_3$/Me	$SrTiO_3$/Me	$BaFeO_3$/Me	$BaCoO_3$/Me	$BaNiO_3$/Me
			Pt substrate		
ΔH_f (eV/at.)	−0.42	−0.41	−0.24	−0.26	0.20
			Au substrate		
ΔH_f (eV/at.)	−0.42	−0.42	−0.24	−0.24	−0.17

Table S3: Formation enthalpy of the supported TPF ($T = 0$ K) according to $8\mathrm{Ba} + 6B + 6\mathrm{O_2} + \mathrm{Pt_{32}} \rightarrow \mathrm{Pt_{32}Ba_8}B_6\mathrm{O_{24}}$

	$BaTiO_3$/Me	$SrTiO_3$/Me	$BaFeO_3$/Me	$BaCoO_3$/Me	$BaNiO_3$/Me
			Pt substrate		
ΔH_f (eV/f.u.)	−1.52	−1.56	−0.94	−0.99	−0.79
			Au substrate		
ΔH_f (eV/f.u.)	−1.48	−1.50	−0.91	−0.92	−0.73

Table S4: Formation enthalpy of the supported SHS ($T = 0$ K) according to $\mathrm{Ba} + 4B + 3\mathrm{O_2} + \mathrm{Pt_{32}} \rightarrow \mathrm{Pt_{32}Ba}B_4\mathrm{O_6}$

	$BaTiO_3$/Me	$SrTiO_3$/Me	$BaFeO_3$/Me	$BaCoO_3$/Me	$BaNiO_3$/Me
			Pt substrate		
ΔH_f (eV/at.)	−0.84	−0.83	−0.28	−0.31	−0.11
			Au substrate		
ΔH_f (eV/at.)	−0.72	−0.72	−0.24	−0.28	−0.09

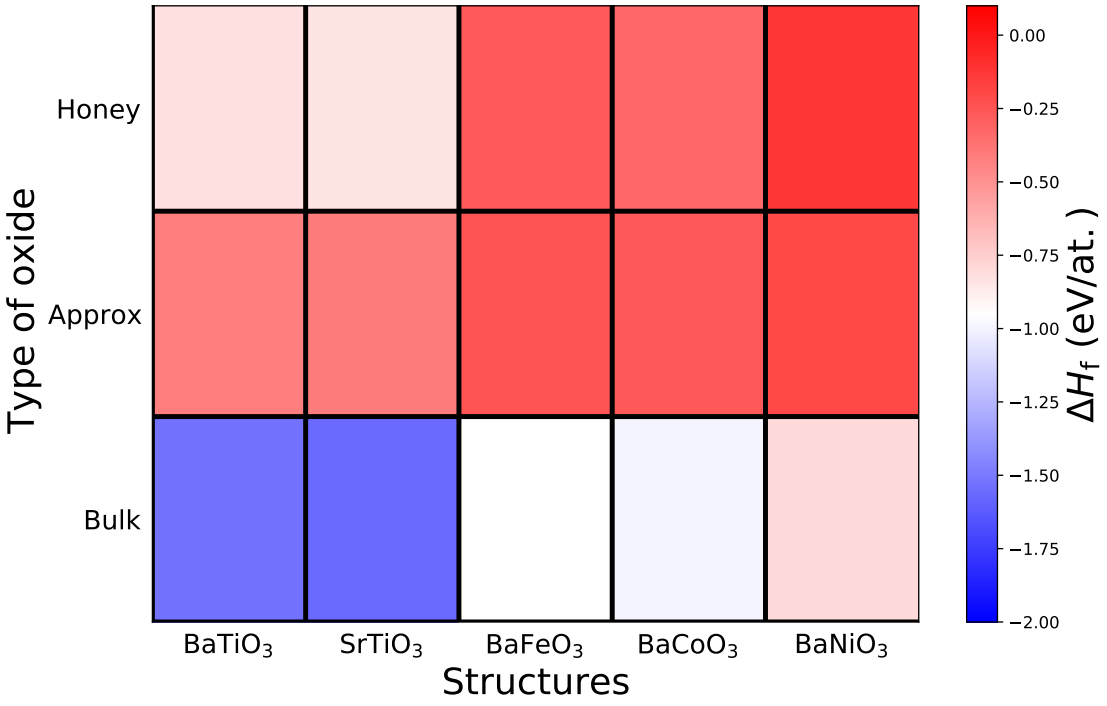

Figure S3: Formation enthalpies ($T = 0$ K), according to r1, r2, r3 with the Pt substrate.

Properties of OQA films

Table S5: BaBO$_3$/Me(111) systems (B = Ti, V, Cr, Mn, Fe, Co, Ni and Me = Pt, Pd, Au) : film rumplings (R), Bader charges (Q), enthalpies of formation at 0 K (ΔH_f), adhesion energies (E_adh), lattice mismatch, work function differences (ΔW), dipole moments in the surface normal direction z (D_z), and atomic magnetic moments (m). Bader charges are expressed in units of elementary charge (e), positive charges indicate cations. Q_Me corresponds to the average charge of Me atoms in the topmost metal layer of Me(111). Q_B and m_B stand for Bader charge and magnetic moment of atom B of ABO$_3$, respectively. MS stands for the ground-state spin order (NM ≡ non-magnetic, FM ≡ ferromagnetic, and AFM ≡ anti ferromagnetic).

	$BaTiO_3$	$BaVO_3$	$BaCrO_3$	$BaMnO_3$	$BaFeO_3$	$BaCoO_3$	$BaNiO_3$
				Freestanding layer			
Q_Ba (e)	1.58	1.60	/	/	1.63	1.63	1.63
Q_B (e)	1.96	1.39	/	/	1.18	1.13	1.05
Q_O (e)	−1.31	−1.13	/	/	−1.07	−1.06	−1.03
m_B (μ_B)	0.2	0.5	/	/	2.5	1.4	0.11
				Pt substrate			
R (Å)	−0.17	−0.27	−0.19	/	−0.06	0.11	0.21
Q_Ba (e)	1.54	1.53	1.50	/	1.52	1.54	1.51
Q_B (e)	1.98	1.71	1.76	/	1.37	1.16	0.94
Q_O (e)	−1.09	−0.94	−0.97	/	−0.97	−0.98	−0.95
Q_Pt (e)	−0.10	−0.12	−0.11	/	−0.07	−0.03	0.00
ΔH_f (eV)	−0.42	−0.36	−0.15	/	−0.24	−0.26	−0.21
E_adh (meV/Å^2)	−81.73	−81.56	/	/	−50.96	−67.53	−50.76
mismatch (%)	32.20	25.75	/	/	31.20	26.06	27.07
ΔW (eV)	2.01	2.15	2.20	/	2.18	2.25	2.25
D_z (eÅ)	−2.12	−2.37	−2.85	/	−2.44	−2.62	−2.76
m_B (μ_B)	0.0	0.0	0.03	/	3.32	0.04	0.67
MS	NM	NM	AFM	/	FM	AFM	AFM
				Pd substrate			
R (Å)	−0.11	−0.23	−0.18	0.03	0.07	0.25	0.31
Q_Ba (e)	1.51	1.50	1.48	1.51	1.50	1.51	1.49
Q_B (e)	1.96	1.68	1.73	1.57	1.51	1.21	0.96
Q_O (e)	−1.12	−0.95	−0.97	−1.04	−0.94	−0.98	−0.91
Q_Pd (e)	−0.07	−0.09	−0.08	−0.04	−0.05	−0.02	0.01
ΔH_f (eV)	−0.41	−0.35	−0.14	−0.23	−0.24	−0.26	−0.20
E_adh (meV/Å^2)	−78.08	−75.99	/	/	−50.06	−68.46	−55.29
mismatch (%)	30.95	24.21	/	/	29.94	24.70	25.74
ΔW (eV)	2.16	2.19	2.21	2.21	2.20	2.22	2.20
D_z (eÅ)	−1.85	−2.07	−2.30	−2.30	−2.21	−2.56	−2.29
m_B (μ_B)	0.0	0.0	0.59	0.92	3.58	2.57	0.03
MS	NM	NM	AFM	AFM	FM	FM	AFM
				Au substrate			
R (Å)	−0.16	−0.36	/	−0.03	0.03	0.17	0.21
Q_Ba (e)	1.58	1.57	/	1.57	1.56	1.55	1.54
Q_B (e)	2.00	1.74	/	1.57	1.31	1.19	0.92
Q_O (e)	−1.14	−0.97	/	−1.09	−1.03	−1.00	−0.99
Q_Au (e)	−0.08	−0.11	/	−0.07	−0.06	−0.04	0.00
ΔH_f (eV)	−0.42	−0.35	/	−0.24	−0.24	−0.24	−0.18
E_adh (meV/Å^2)	−76.72	−68.72	/	/	−45.03	−49.00	−32.54
mismatch (%)	38.22	32.18	/	/	37.32	32.62	33.55
ΔW (eV)	2.12	2.15	/	2.15	2.17	2.17	2.20
D_z (eÅ)	−1.58	−1.94	/	−1.95	−2.25	−2.13	−2.46
m_B (μ_B)	0.0	0.0	/	1.17	3.40	2.76	0.05
MS	NM	NM	/	AFM	FM	FM	AFM

Table S6: SrBO$_3$/Me(111) systems (B = Ti, V, Cr, Mn, Fe, Co, Ni and Me = Pt, Pd, Au) : film rumplings (R), Bader charges (Q), enthalpies of formation at 0 K (ΔH_f), adhesion energies (E_adh), lattice mismatch, work function differences (ΔW), dipole moments in the surface normal direction z (D_z), and atomic magnetic moments (m). Bader charges are expressed in units of elementary charge (e), positive charges indicate cations. Q_Me corresponds to the average charge of Me atoms in the topmost metal layer of Me(111). Q_B and m_B stand for Bader charge and magnetic moment of atom B of ABO$_3$, respectively. MS stands for the ground-state spin order (NM ≡ non-magnetic, FM ≡ ferromagnetic, and AFM ≡ anti ferromagnetic).

	$SrTiO_3$	$SrVO_3$	$SrCrO_3$	$SrMnO_3$	$SrFeO_3$	$SrCoO_3$	$SrNiO_3$
				Freestanding layer			
Q_Sr (e)	1.60	1.61	1.63	1.62	/	/	1.61
Q_B (e)	1.90	1.44	1.61	1.60	/	/	1.12
Q_O (e)	−1.30	−1.15	−1.14	−1.21	/	/	−1.04
m_B (μ_B)	0.1	0.4	1.39	0.0	/	/	0.9
				Pt substrate			
R (Å)	−0.22	−0.29	−0.25	−0.05	−0.12	−0.05	0.20
Q_Sr (e)	1.56	1.56	1.54	1.56	1.57	1.57	1.57
Q_B (e)	1.99	1.71	1.77	1.55	1.36	1.25	0.92
Q_O (e)	−1.10	−0.95	−0.98	−1.05	−0.98	−0.99	−0.94
Q_Pt (e)	−0.10	−0.12	−0.11	−0.06	−0.07	−0.05	−0.04
ΔH_f (eV)	−0.40	−0.35	−0.14	−0.24	−0.23	−0.25	0.87
E_adh (meV/Å^2)	−75.8	−74.74	−50.28	−51.8	/	/	−49.22
mismatch (%)	37.16	39.84	31.56	40.27	/	/	42.14
ΔW (eV)	2.15	2.20	2.19	2.16	2.19	2.21	2.19
D_z (eÅ)	−1.65	−2.20	−2.43	−1.65	−1.93	−1.72	−2.11
m_B (μ_B)	0.00	0.00	1.17	3.41	0.14	0.04	0.32
MS	NM	NM	FM	FM	AFM	AFM	AFM
				Pd substrate			
R (Å)	−0.14	−0.27	−0.23	0.1	0.05	0.23	0.23
Q_Sr (e)	1.56	1.53	1.56	1.55	1.53	1.54	1.54
Q_B (e)	1.97	1.69	1.69	1.54	1.35	1.20	1.04
Q_O (e)	−1.13	−0.97	−1.04	−1.06	−0.99	−1.00	−0.95
Q_Pd (e)	−0.02	−0.10	−0.07	−0.05	−0.05	−0.03	−0.03
ΔH_f (eV)	−0.41	−0.34	−0.13	−0.24	−0.23	−0.26	−0.19
E_adh (meV/Å^2)	−74.22	−72.49	−45.19	−58.1	/	/	−38.49
mismatch (%)	36.01	38.74	30.31	39.18	/	/	41.08
ΔW (eV)	2.14	2.14	2.15	2.20	2.16	2.19	2.20
D_z (eÅ)	−1.45	−1.61	−1.89	−1.30	−2.09	−2.16	−2.13
m_B (μ_B)	0.00	0.00	1.23	0.00	3.76	2.59	0.48
MS	NM	NM	FM	FM	FM	FM	FM
				Au substrate			
R (Å)	−0.19	−0.39	/	0.07	−0.07	0.11	0.20
Q_Sr (e)	1.58	1.57	/	1.57	1.57	1.57	1.56
Q_B (e)	1.99	1.73	/	1.57	1.34	1.12	0.95
Q_O (e)	−1.16	−0.97	/	−1.11	−1.01	−1.03	−1.02
Q_Au (e)	−0.08	−0.11	/	−0.03	−0.05	−0.02	0.00
ΔH_f (eV)	−0.42	−0.36	/	−0.24	−0.22	−0.23	−0.18
E_adh (meV/Å^2)	−75.56	−74.64	/	−50.43	/	/	−24.93
mismatch (%)	42.74	45.19	/	45.58	/	/	47.28
ΔW (eV)	2.10	2.13	/	2.14	2.12	2.14	2.15
D_z (eÅ)	−1.28	−1.60	/	−1.58	−1.58	−1.67	−1.92
m_B (μ_B)	0.00	0.00	/	0.00	1.50	0.11	0.44
MS	NM	NM	/	AFM	AFM	AFM	FM

Table S7: CaBO$_3$/Me(111) systems (B = Ti, V, Cr, Mn, Fe, Co, Ni and Me = Pt, Pd, Au) : film rumplings (R), Bader charges (Q), enthalpies of formation at 0K (H_{for}), adhesion energies (E_{madh}), lattice mismatch, work function differences (ΔW), dipole moments in the z direction (D_z), and atomic magnetic moments (m). Bader charges are expressed in units of elementary charge (e), positive charges indicate cations. Q_{Me} corresponds to the average charge of Me atoms in the topmost metal layer of Me(111). Q_B and m_B stands for Bade charge and magnetic moment of atom B of ABO$_3$. MS stands for the ground-state spin order

	$CaTiO_3$	$CaVO_3$	$CaCrO_3$	$CaMnO_3$	$CaFeO_3$	$CaCoO_3$	$CaNiO_3$
				Freestanding layer			
Q_{Ca} (e)	1.55	/	/	1.57	/	1.58	/
Q_B (e)	1.94	/	/	1.64	/	1.32	/
Q_{O} (e)	−1.29	/	/	−1.20	/	−1.10	/
m_B (μ_{B})	0.3	/	/	0.0	/	2.3	/
				Pt substrate			
R (Å)	−0.24	−0.35	−0.31	/	−0.04	0.07	0.14
Q_{Ca} (e)	1.53	1.53	1.51	/	1.54	1.54	1.54
Q_B (e)	2.01	1.73	1.78	/	1.40	1.25	1.05
Q_{O} (e)	−1.10	−0.94	−0.97	/	−0.98	−0.98	−0.93
Q_{Pt} (e)	−0.09	−0.12	0.11	/	−0.06	−0.05	−0.04
ΔH_{f} (eV)	−0.40	−0.34	−0.13	/	−0.23	−0.25	−0.19
E_{adh} (meV/Å^2)	−78.59	/	/	/	/	−61.11	/
mismatch (%)	43.55	/	/	/	/	45.49	/
ΔW (eV)	2.11	2.11	2.15	/	2.16	2.15	2.14
D_z (eÅ)	−1.25	−1.62	−1.82	/	−1.90	−1.83	−1.68
m_B (μ_{B})	0.0	0.0	1.55	/	0.22	0.11	1.44
MS	NM	NM	FM	/	AFM	AFM	FM
				Pd substrate			
R (Å)	−0.17	−0.30	−0.32	0.07	−0.02	0.07	0.29
Q_{Ca} (e)	1.53	1.49	1.49	1.53	1.50	1.51	1.51
Q_B (e)	1.98	1.70	1.72	1.54	1.36	1.25	1.01
Q_{O} (e)	−1.13	−0.97	−0.99	−1.06	−1.00	−1.02	−0.95
Q_{Pd} (e)	−0.07	−0.09	−0.08	−0.02	−0.04	−0.03	−0.02
ΔH_{f} (eV)	−0.40	−0.34	−0.14	−0.24	−0.23	−0.24	−0.20
E_{adh} (meV/Å^2)	−81.14	/	/	/	/	−64.81	/
mismatch (%)	42.51	/	/	/	/	44.49	/
ΔW (eV)	2.10	2.11	2.12	2.16	2.12	2.13	2.12
D_z (eÅ)	−1.00	−1.13	−1.06	−0.89	−1.26	−1.37	−1.35
m_B (μ_{B})	0.00	0.00	1.14	0.00	0.26	0.12	1.45
MS	NM	NM	FM	FM	AFM	AFM	AFM
				Au substrate			
R (Å)	−0.16	−0.40	−0.36	0.06	0.04	0.14	0.23
Q_{Ca} (e)	1.55	1.54	1.53	1.55	1.54	1.54	1.53
Q_B (e)	2.03	1.75	1.80	1.59	1.38	1.15	1.02
Q_{O} (e)	−1.16	−0.96	−1.02	−1.07	−1.05	−1.06	−1.00
Q_{Au} (e)	−0.08	−0.11	−0.09	−0.04	−0.03	0.00	0.00
ΔH_{f} (eV)	−0.40	−0.34	−0.12	−0.25	−0.23	−0.23	−0.18
E_{adh} (meV/Å^2)	−68.16	/	/	−61.77	/	−41.80	/
mismatch (%)	48.56	/	/	47.51	/	50.33	/
ΔW (eV)	2.07	2.07	2.07	2.11	2.08	2.11	2.14
D_z (eÅ)	−0.93	−1.03	−0.92	−0.73	−1.11	−1.39	−1.68
m_B (μ_{B})	0.00	0.00	0.65	0.00	0.17	1.33	1.24
MS	NM	NM	AFM	AFM	AFM	AFM	FM

Gibbs free energies

(a) $BaTiO_3$/Pt(111)

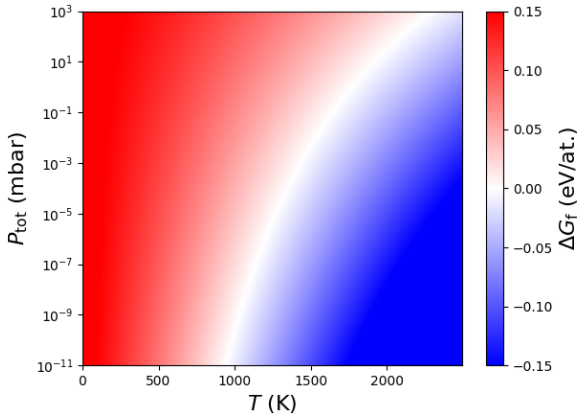

(b) $BaTiO_3$/Au(111)

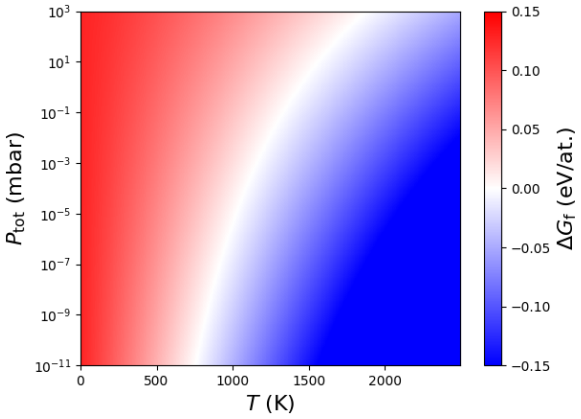

(c) $SrTiO_3$/Pt(111)

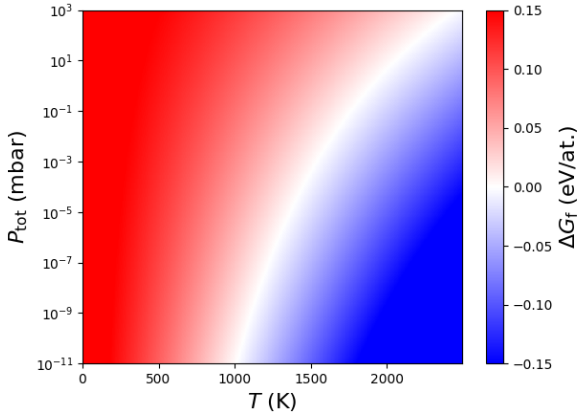

(d) $SrTiO_3$/Au(111)

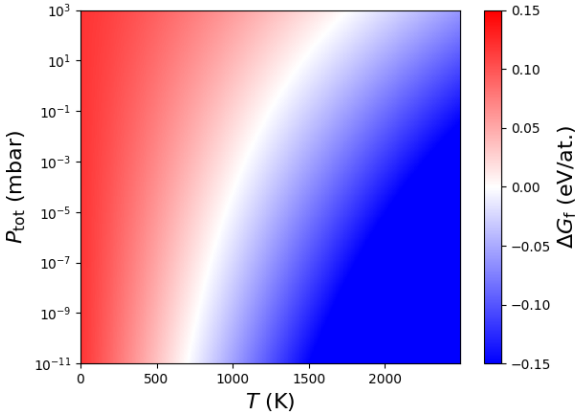

(e) $BaFeO_3$/Pt(111)

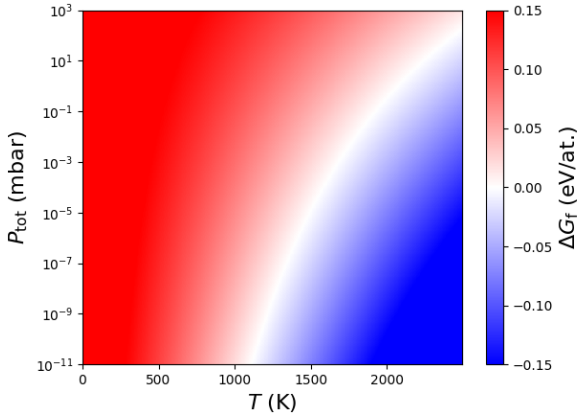

(f) $BaFeO_3$/Au(111)

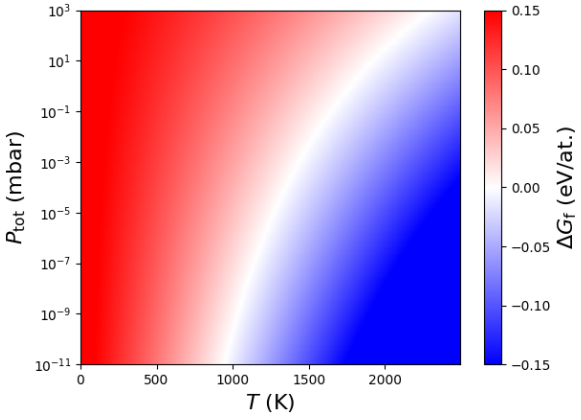

Figure S4: Gibbs free energy of the following reaction : 15 $Pt_{32}Ba_8B_6O_{24}$ → 4 $Pt_{120}Ba_5B_4O_{12}$ + 74 $BaBO_3$ + 45 O_2 + 26 Ba. The thick ABO_3 film is more stable than the OQA in the red region. The OQA is more stable than the thick ABO_3 film in the blue region.

(a) $BaCoO_3$/Pt(111)

(b) $BaCoO_3$/Au(111)

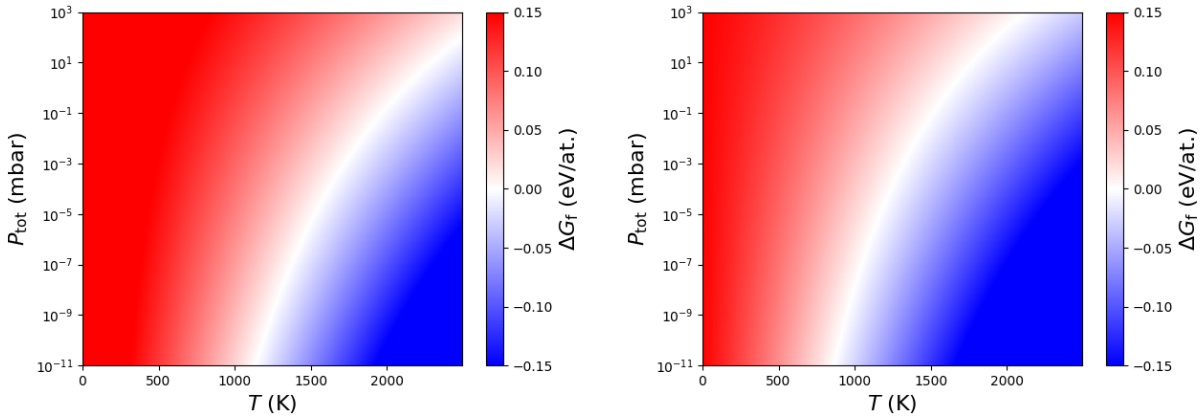

(c) $BaNiO_3$/Pt(111)

(d) $BaNiO_3$/Au(111)

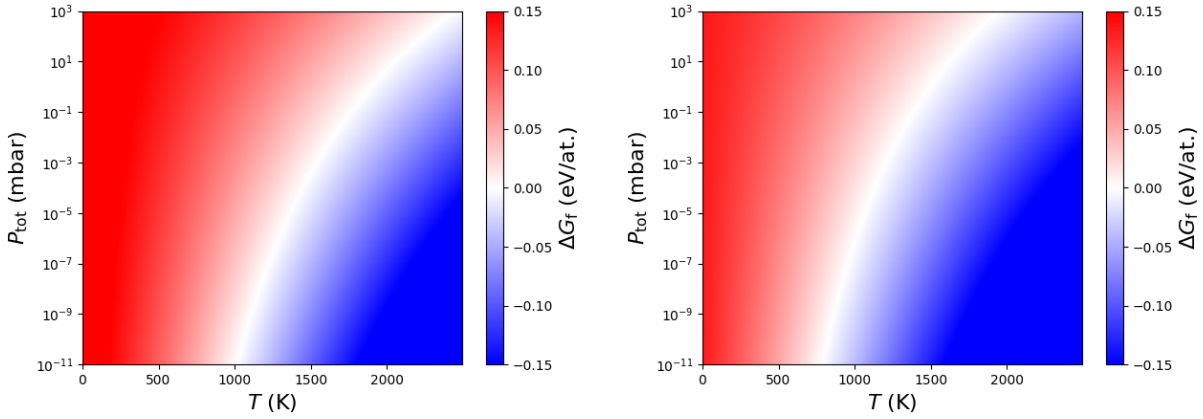

Figure S5: Gibbs free energy of the following reaction : 15 $Pt_{32}Ba_8B_6O_{24}$ → 4 $Pt_{120}Ba_5B_4O_{12}$ + 74 $BaBO_3$ + 45 O_2 + 26 Ba. The thick ABO_3 film is more stable than the OQA in the red region. The OQA is more stable than the thick ABO_3 film in the blue region.

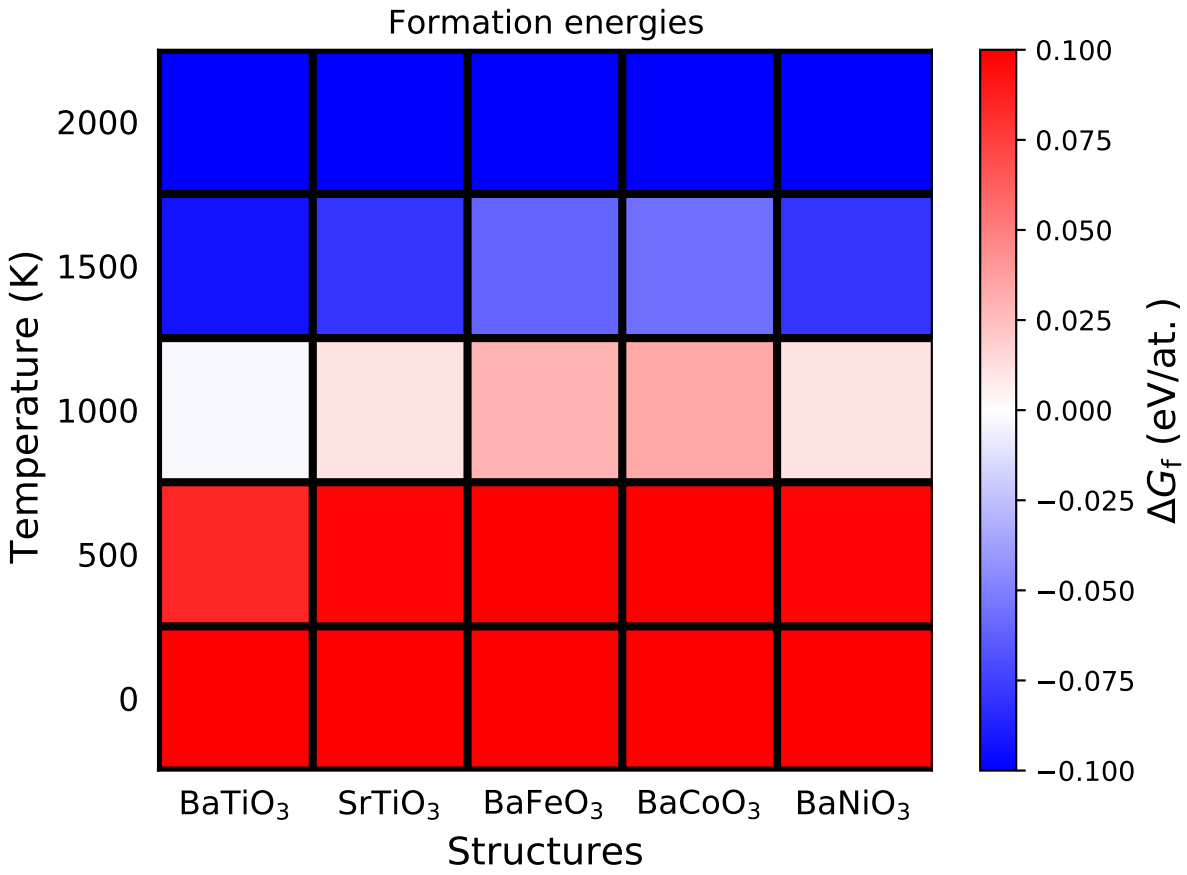

Figure S6: Gibbs free energy corresponding to the following reaction : 15 $Pt_{32}Ba_8B_6O_{24}$ → 4 $Pt_{120}Ba_5B_4O_{12}$ + 74 $BaBO_3$ + 45 O_2 + 26 Ba ($P = 10^{-10}$ mbar).

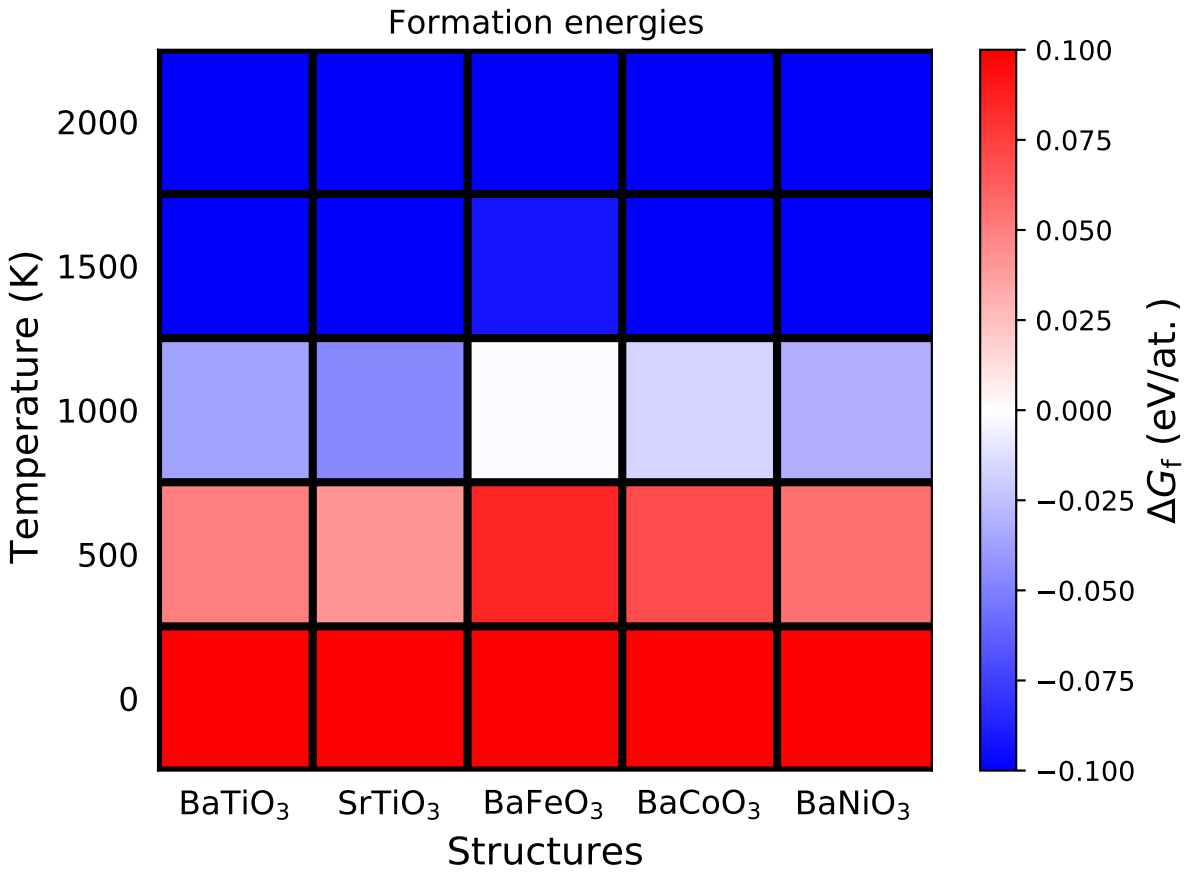

Figure S7: Gibbs free energy corresponding to the following reaction : 15 $Au_{32}Ba_8B_6O_{24} \rightarrow$ 4 $Au_{120}Ba_5B_4O_{12}$ + 74 $BaBO_3$ + 45 O_2 + 26 Ba ($P = 10^{-10}$ mbar).

(a) $BaTiO_3$/Pt(111)

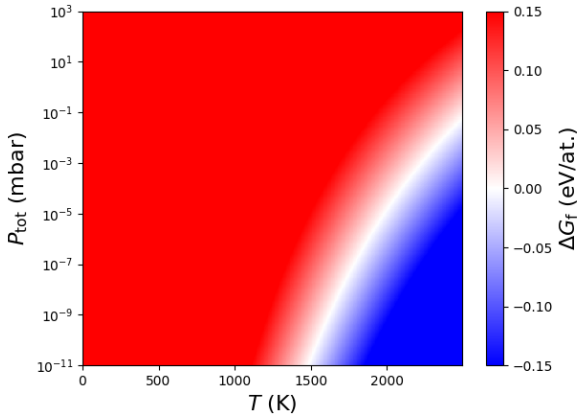

(b) $BaTiO_3$/Au(111)

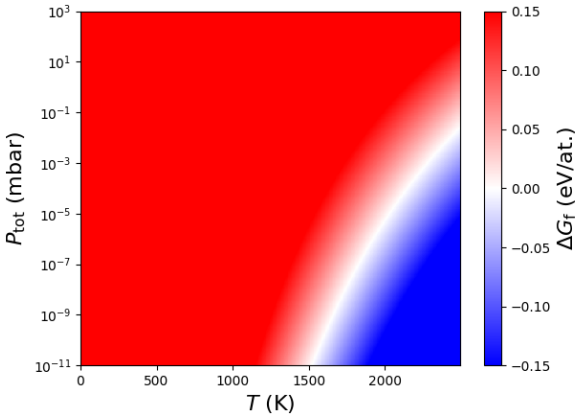

(c) $SrTiO_3$/Pt(111)

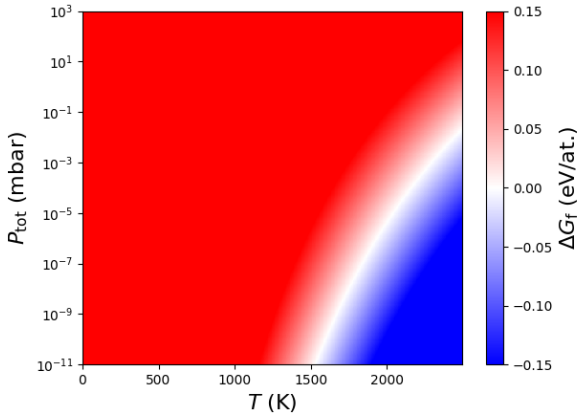

(d) $SrTiO_3$/Au(111)

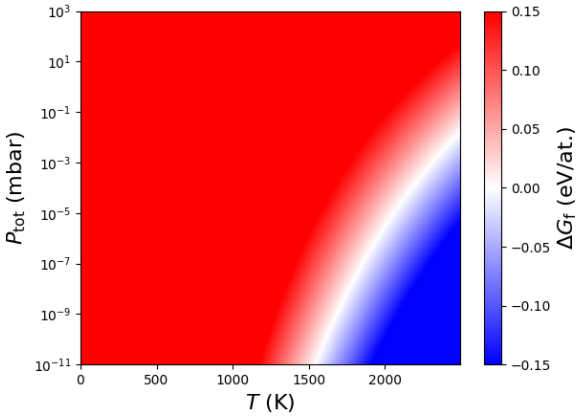

(e) $BaFeO_3$/Pt(111)

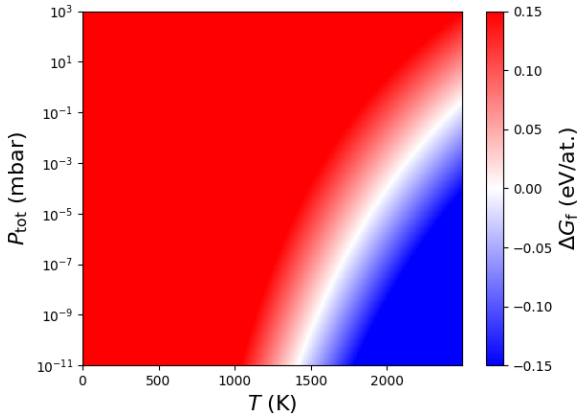

(f) $BaFeO_3$/Au(111)

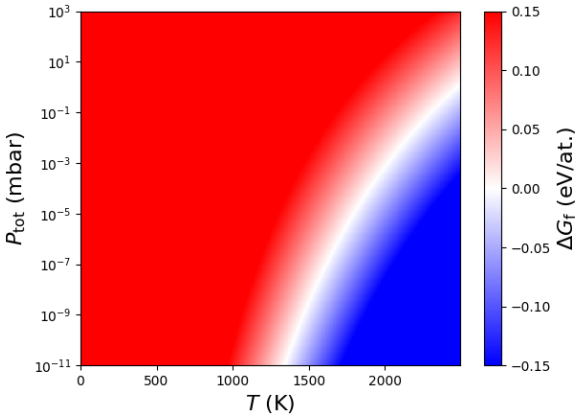

Figure S8: Gibbs free energy of the following reaction : $Pt_{32}Ba_8B_6O_{24} \rightarrow Pt_{32}BaB_4O_6$ + 2 $BaBO_3$ + 6 O_2 + 5/2 Ba. The thick ABO_3 film is more stable than the SHS in the red region. The SHS is more stable than the thick ABO_3 film in the blue region.

(a) $BaCoO_3$/Pt(111)

(b) $BaCoO_3$/Au(111)

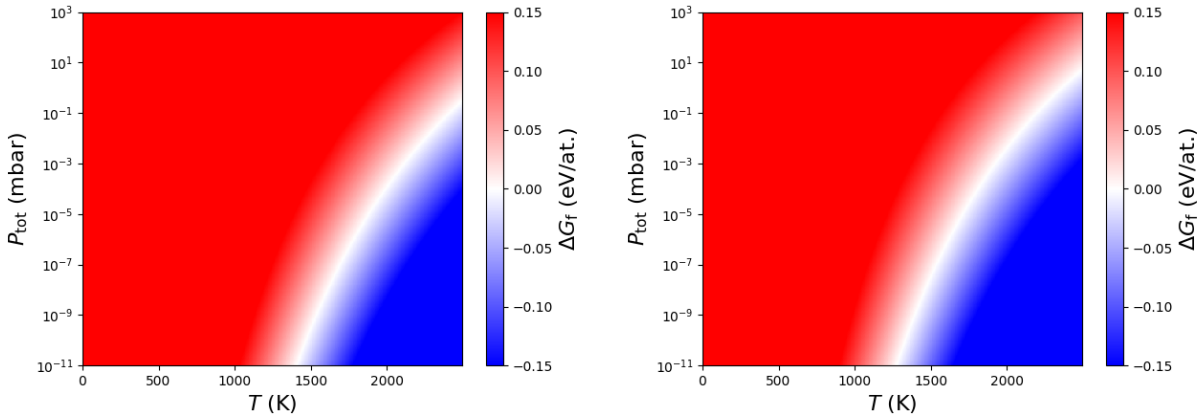

(c) $BaNiO_3$/Pt(111)

(d) $BaNiO_3$/Au(111)

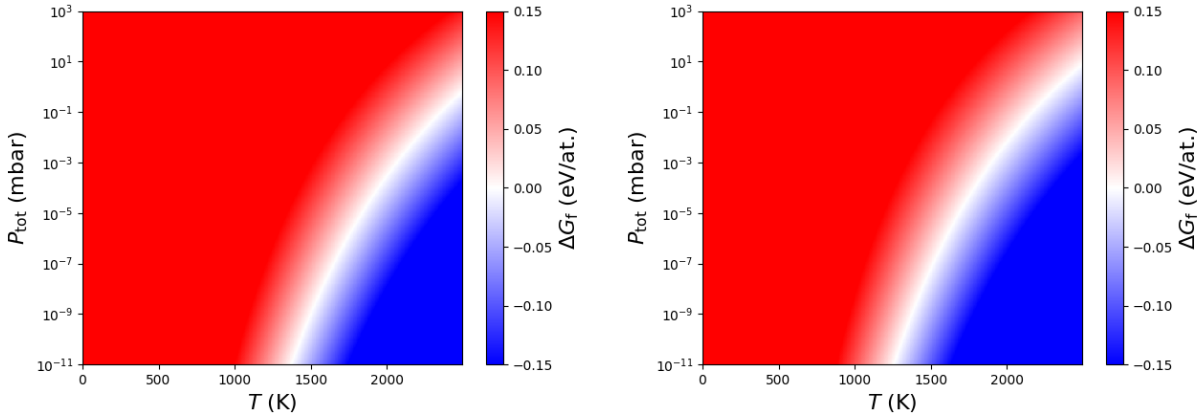

Figure S9: Gibbs free energy of the following reaction : $Pt_{32}Ba_8B_6O_{24} \rightarrow Pt_{32}BaB_4O_6 + 2\ BaBO_3 + 6\ O_2 + 5/2$ Ba. The thick ABO_3 film is more stable than the SHS in the red region. The SHS is more stable than the thick ABO_3 film in the blue region.

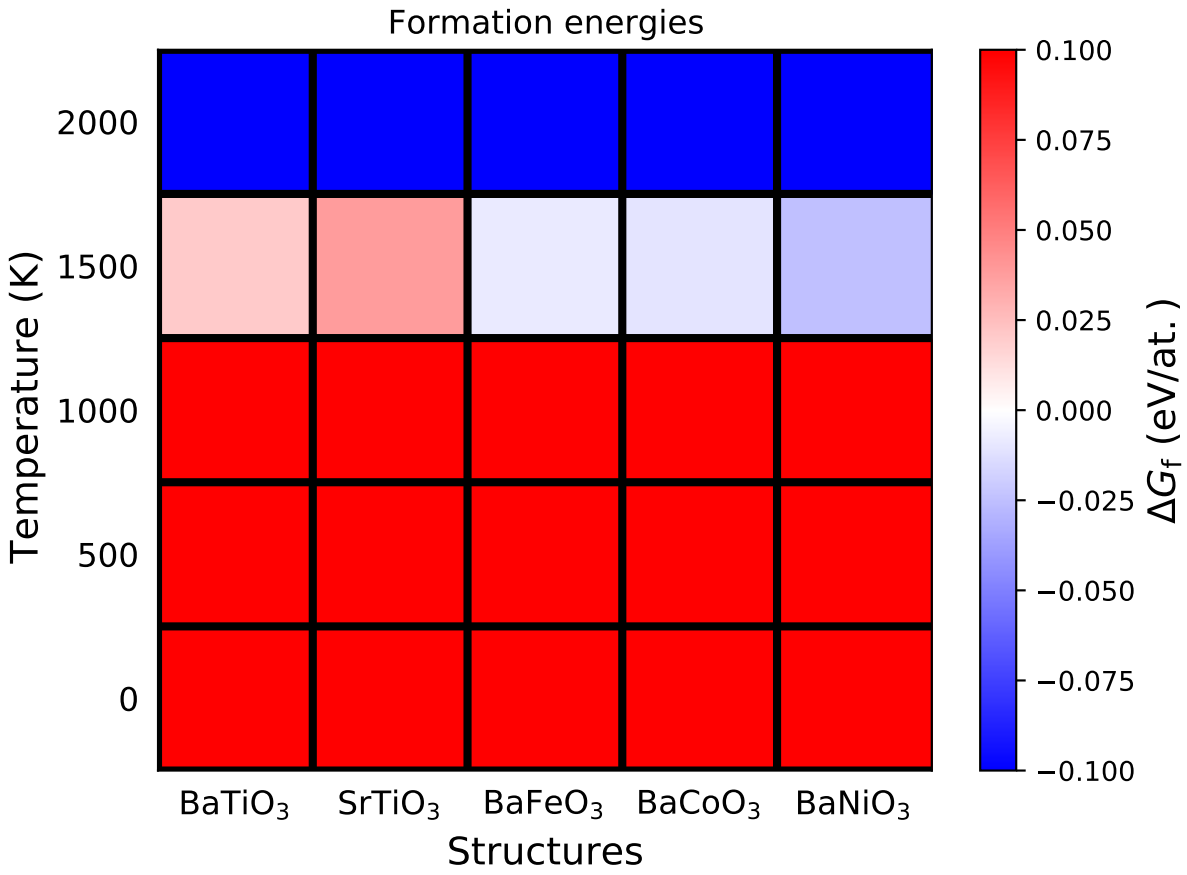

Figure S10: Gibbs free energy corresponding to the following reaction : $Pt_{32}Ba_8B_6O_{24} \rightarrow Pt_{32}BaB_4O_6$ + 2 $BaBO_3$ + 6 O_2 + 5/2 Ba ($P = 10^{-10}$ mbar).

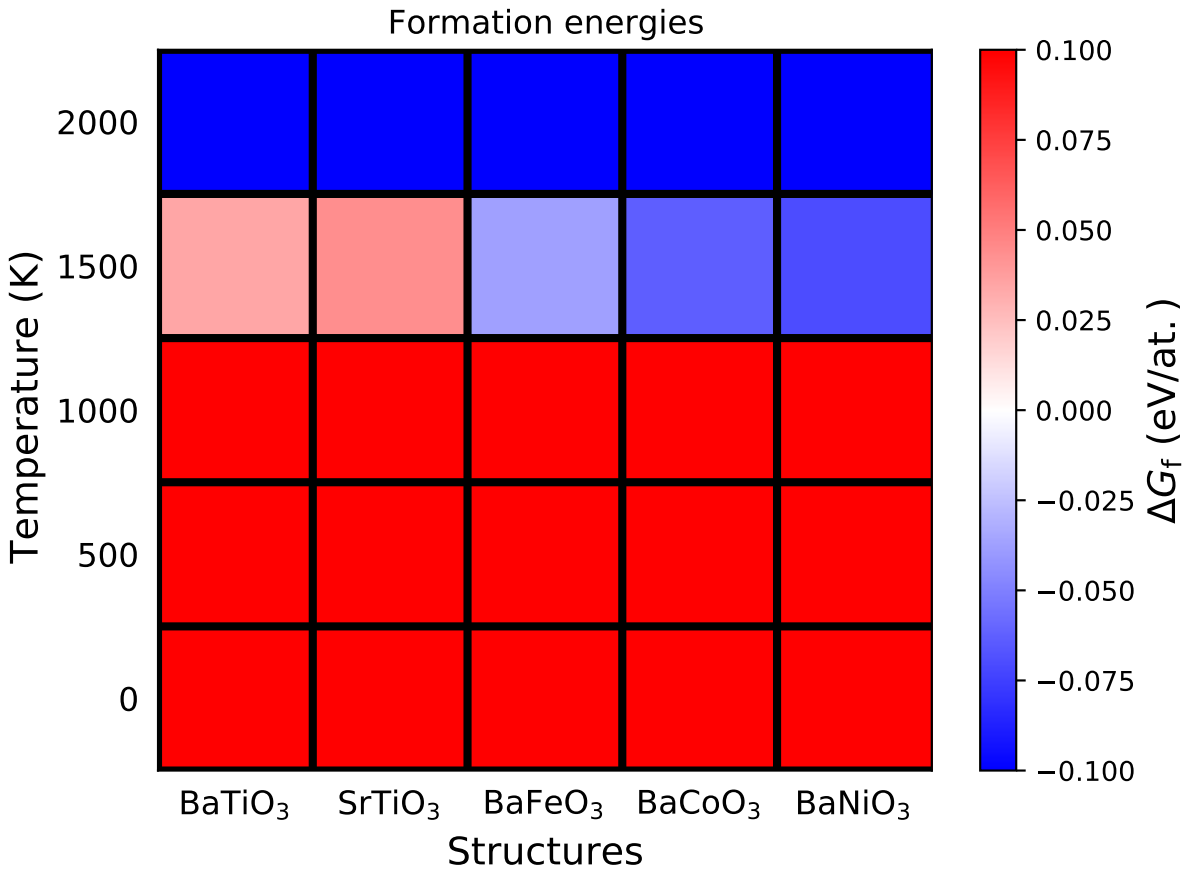

Figure S11: Gibbs free energy corresponding to the following reaction : $Au_{32}Ba_8B_6O_{24} \rightarrow Au_{32}BaB_4O_6 + 2\ BaBO_3 + 6\ O_2 + 5/2$ Ba ($P = 10^{-10}$ mbar).

Atomic structures of OQAs

Table S8: Average $A-\mathrm{O}$, $B-\mathrm{O}$, $A-\mathrm{Me}$, and $B-\mathrm{Me}$ bond lengths, as well as the rumplings and average O$-B-$O angles in all structures.

	$BaTiO_3$	$BaVO_3$	$BaCrO_3$	$BaMnO_3$	$BaFeO_3$	$BaCoO_3$	$BaNiO_3$
				Freestanding layer			
$B-$O (Å)	1.79	1.74	/	/	1.71	1.73	1.72
Ba$-$O (Å)	2.64	2.64	/	/	2.7	2.55	2.63
O$-B-$O angle (°)	120.0	120.0	/	/	120.0	120.0	120.0
				Pt substrate			
$B-$O (Å)	1.84	1.74	1.72	/	1.81	1.84	1.88
Ba$-$O (Å)	2.7	2.78	2.78	/	2.66	2.67	2.7
$B-$Pt (Å)	3.06	2.82	2.9	/	2.91	2.98	2.88
Ba$-$Pt (Å)	3.48	3.43	3.52	/	3.52	3.52	3.55
O$-B-$O angle (°)	112.2	111.0	113.4	/	115.4	117.3	117.5
				Pd substrate			
$B-$O (Å)	1.83	1.74	1.71	1.77	1.79	1.82	1.87
$B-$Pd (Å)	3.02	2.95	2.91	3.02	2.92	2.99	2.87
Ba$-$O (Å)	2.67	2.75	2.74	2.68	2.65	2.63	2.74
Ba$-$Pd (Å)	3.51	3.5	3.49	3.48	3.57	3.59	3.55
O$-B-$O angle (°)	113.8	111.4	114.3	117.3	116.9	118.8	118.1
				Au substrate			
$B-$O (Å)	1.82	1.72	/	1.79	1.77	1.79	1.86
$B-$Au (Å)	3.09	2.99	/	3.03	2.93	2.93	2.94
Ba$-$O (Å)	2.74	2.76	/	2.72	2.7	2.7	2.71
Ba$-$Au (Å)	3.54	3.42	/	3.55	3.54	3.55	3.56
O$-B-$O angle (°)	115.3	112.2	/	118.8	118.5	119.7	118.9
	$SrTiO_3$	$SrVO_3$	$SrCrO_3$	$SrMnO_3$	$SrFeO_3$	$SrCoO_3$	$SrNiO_3$
				Freestanding layer			
$B-$O (Å)	1.79	1.74	1.82	1.76	/	/	1.72
Sr$-$O (Å)	2.46	2.58	2.43	2.5	/	/	2.53
O$-B-$O angle (°)	120.0	120.0	120.0	120.0	/	/	120.0
				Pt substrate			
$B-$O (Å)	1.85	1.75	1.73	1.86	1.82	1.85	1.84
$B-$Pt (Å)	3.06	2.98	2.91	3.02	2.91	2.97	2.95
Sr$-$O (Å)	2.55	2.69	2.67	2.5	2.54	2.53	2.49
Sr$-$Pt (Å)	3.34	3.27	3.27	3.34	3.31	3.34	3.33
O$-B-$O angle (°)	113.6	111.6	114.4	118.0	116.2	117.8	118.2
				Pd substrate			
$B-$O (Å)	1.84	1.74	1.77	1.82	1.8	1.82	1.8
$B-$Pd (Å)	3.04	3.01	2.97	3.0	2.92	2.89	2.98
Sr$-$O (Å)	2.51	2.64	2.7	2.47	2.5	2.48	2.49
Sr$-$Pd (Å)	3.31	3.31	3.42	3.29	3.27	3.3	3.3
O$-B-$O angle (°)	114.3	112.5	114.5	118.7	117.6	119.0	118.9
				Au substrate			
$B-$O (Å)	1.83	1.72	/	1.86	1.79	1.85	1.86
$B-$Au (Å)	3.12	3.01	/	3.07	2.93	2.86	2.97
Sr$-$O (Å)	2.54	2.58	/	2.48	2.56	2.51	2.45
Sr$-$Au (Å)	3.29	3.23	/	3.4	3.29	3.32	3.36
O$-B-$O angle (°)	116.0	113.6	/	119.5	119.1	119.7	119.0
	$CaTiO_3$	$CaVO_3$	$CaCrO_3$	$CaMnO_3$	$CaFeO_3$	$CaCoO_3$	$CaNiO_3$
				Freestanding layer			
$B-$O (Å)	1.8	/	/	1.77	/	1.72	/
Ca$-$O (Å)	2.14	/	/	2.26	/	2.26	/
O$-B-$O angle (°)	120.0	/	/	120.0	/	120.0	/
				Pt substrate			
R (Å)	−0.24	−0.35	−0.31	/	−0.17	−0.10	−0.07
$B-$O (Å)	1.86	1.75	1.73	/	1.85	1.88	1.91
$B-$Pt (Å)	3.07	2.96	2.9	/	2.91	2.95	2.95
Ca$-$O (Å)	2.43	2.5	2.46	/	2.42	2.39	2.35
Ca$-$Pt (Å)	3.17	3.13	3.1	/	3.17	3.18	3.19
O$-B-$O angle (°)	115.3	112.5	114.9	/	117.1	118.3	119.0
				Pd substrate			
R (Å)	−0.22	−0.33	−0.30	−0.11	−0.13	−0.06	0.00
$B-$O (Å)	1.84	1.75	1.73	1.85	1.82	1.85	1.78
$B-$Pd (Å)	3.05	3.01	2.92	3.01	2.95	2.94	2.81
Ca$-$O (Å)	2.38	2.5	2.56	2.34	2.35	2.34	2.29
Ca$-$Pd (Å)	3.2	3.12	3.08	3.2	3.16	3.13	3.14
O$-B-$O angle (°)	116.0	113.9	116.2	119.2	118.4	119.0	128.4
				Au substrate			
R (Å)	−0.13	−0.36	−0.26	−0.12	0.01	0.13	0.14
$B-$O (Å)	1.84	1.73	1.73	1.94	1.86	1.92	1.89
$B-$Au (Å)	3.13	3.06	3.04	2.98	2.95	2.85	2.92
Ca$-$O (Å)	2.33	2.32	2.37	2.46	2.39	2.33	2.3
Ca$-$Au (Å)	3.23	3.05	3.08	3.18	3.2	3.2	3.24
O$-B-$O angle (°)	116.8	114.0	117.0	119.3	119.5	119.5	122.4

Size mismatch and rumpling for OQAs

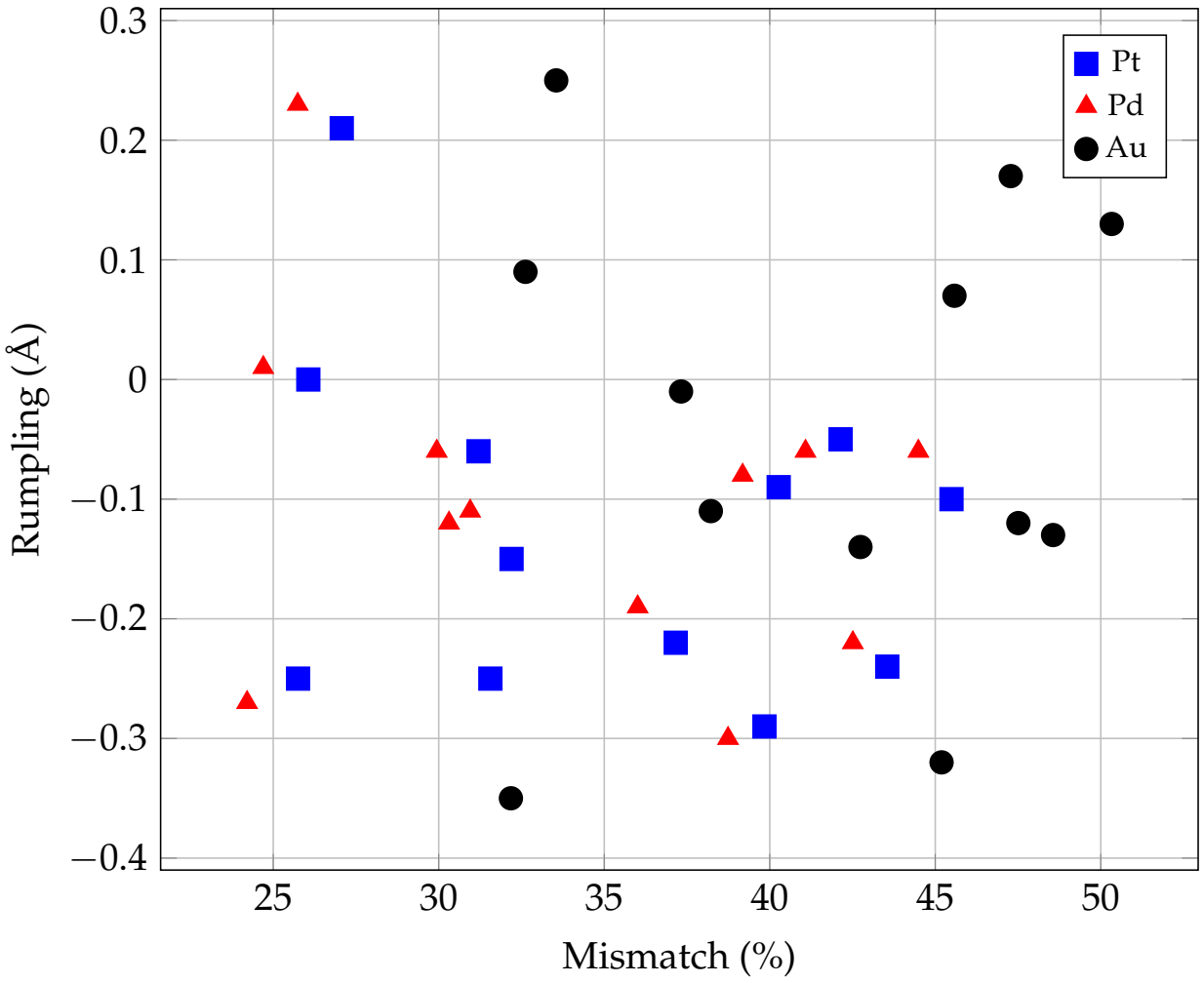

Figure S12: Plot of the rumpling as a function of the size mismatch for selected structures.

Averaged planar differences

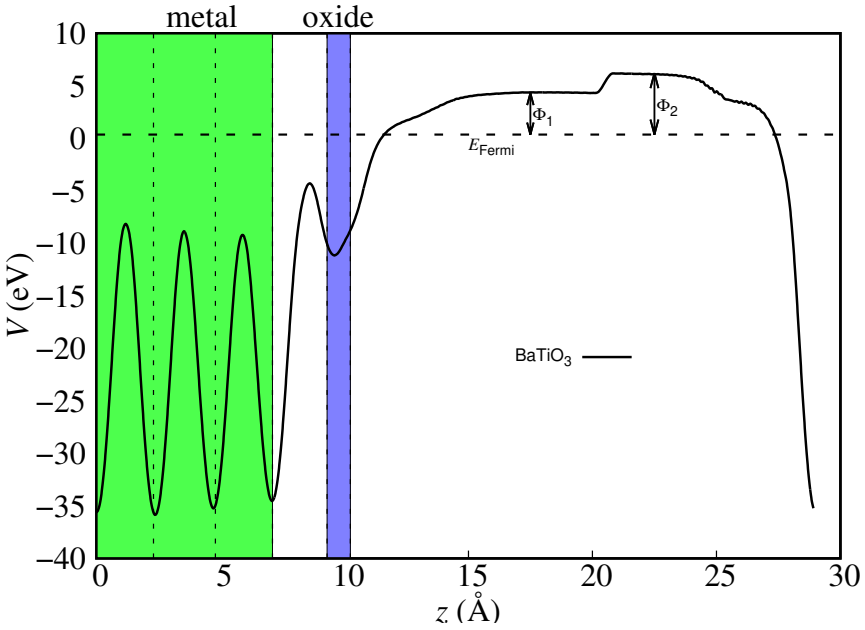

Figure S13: Planar averaged electrostatic potential ($\overline{V}(z) = \frac{1}{A}\int_A V(x,y,z)\mathrm{d}x\mathrm{d}y$, where A is the surface area) for $BaTiO_3$ on Pt. Green band represents the Pt(111) slab and blue stripe indicates the position of the OQA layer. Φ_1 and Φ_2 are the values in the plateau of the average electrostatic potential in the vacuum level (with the Fermi energy as a reference in zero) for the metal-oxide and metal systems, respectivelly.

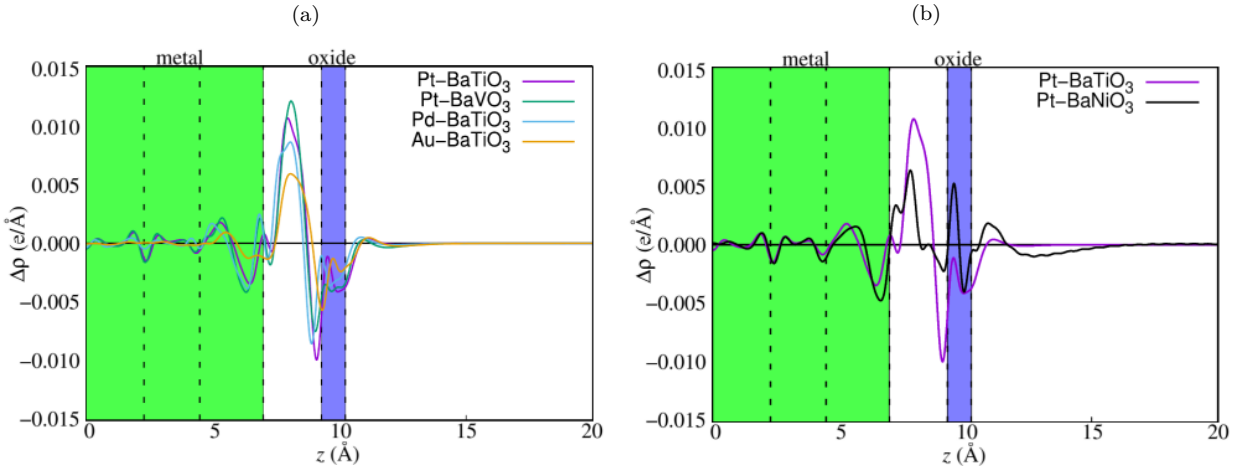

Figure S14: Planar averaged electron charge density differences ($\Delta\rho(z) = \int_A \Delta\rho(x,y,z)\,\mathrm{d}x\mathrm{d}y$, where integration was performed over the area (A) spanned by the surface supercell) for several OQA structures studied in this work. Green represents the Pt(111) slab and blue stripe indicates the position of the OQA layer.

Adhesion energies as a function of size mismatch, rumpling and charge transfer

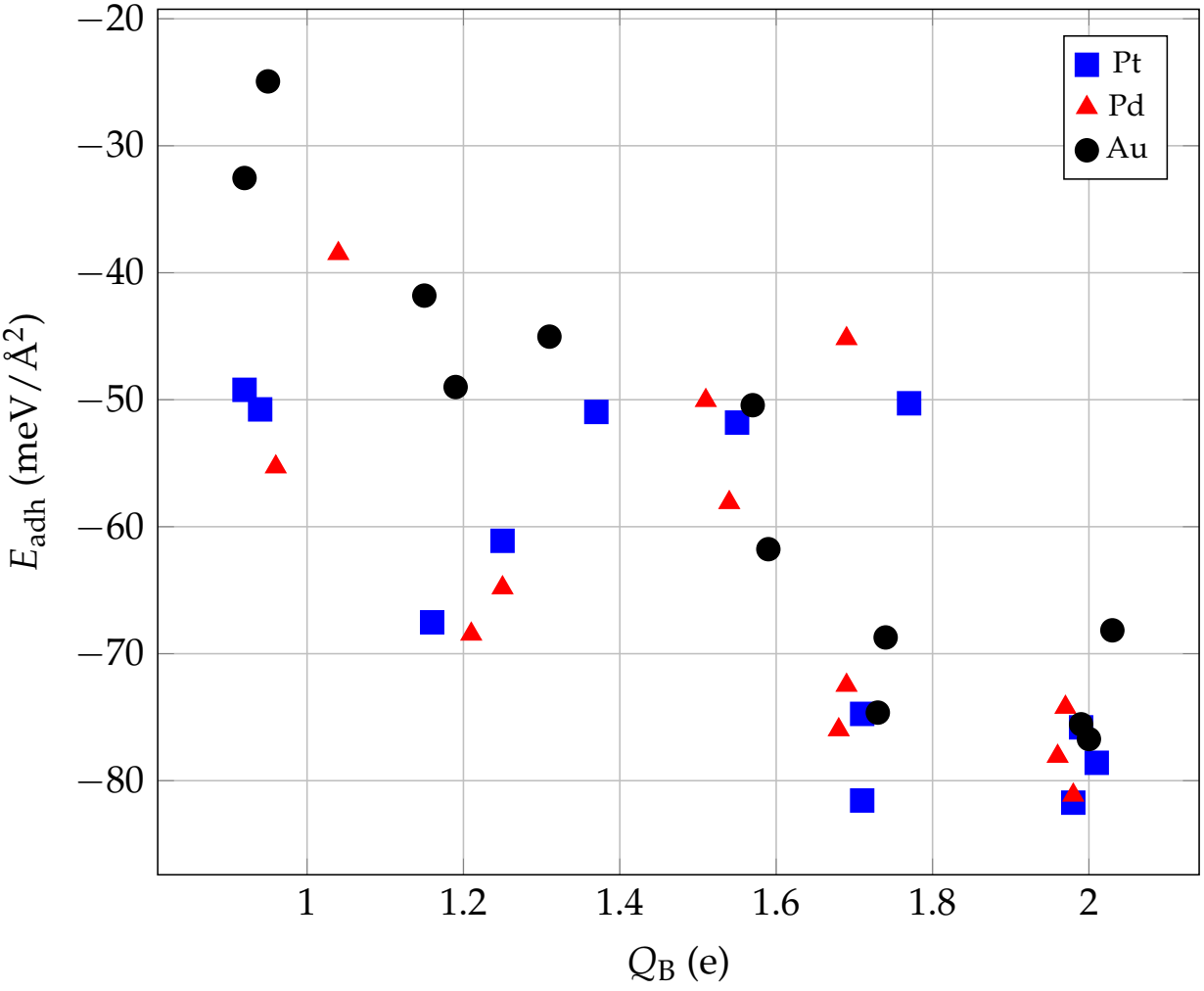

Figure S15: Plot of the adhesion energy (E_{adh}) as a function of the Bader charge of B atom (Q_B).

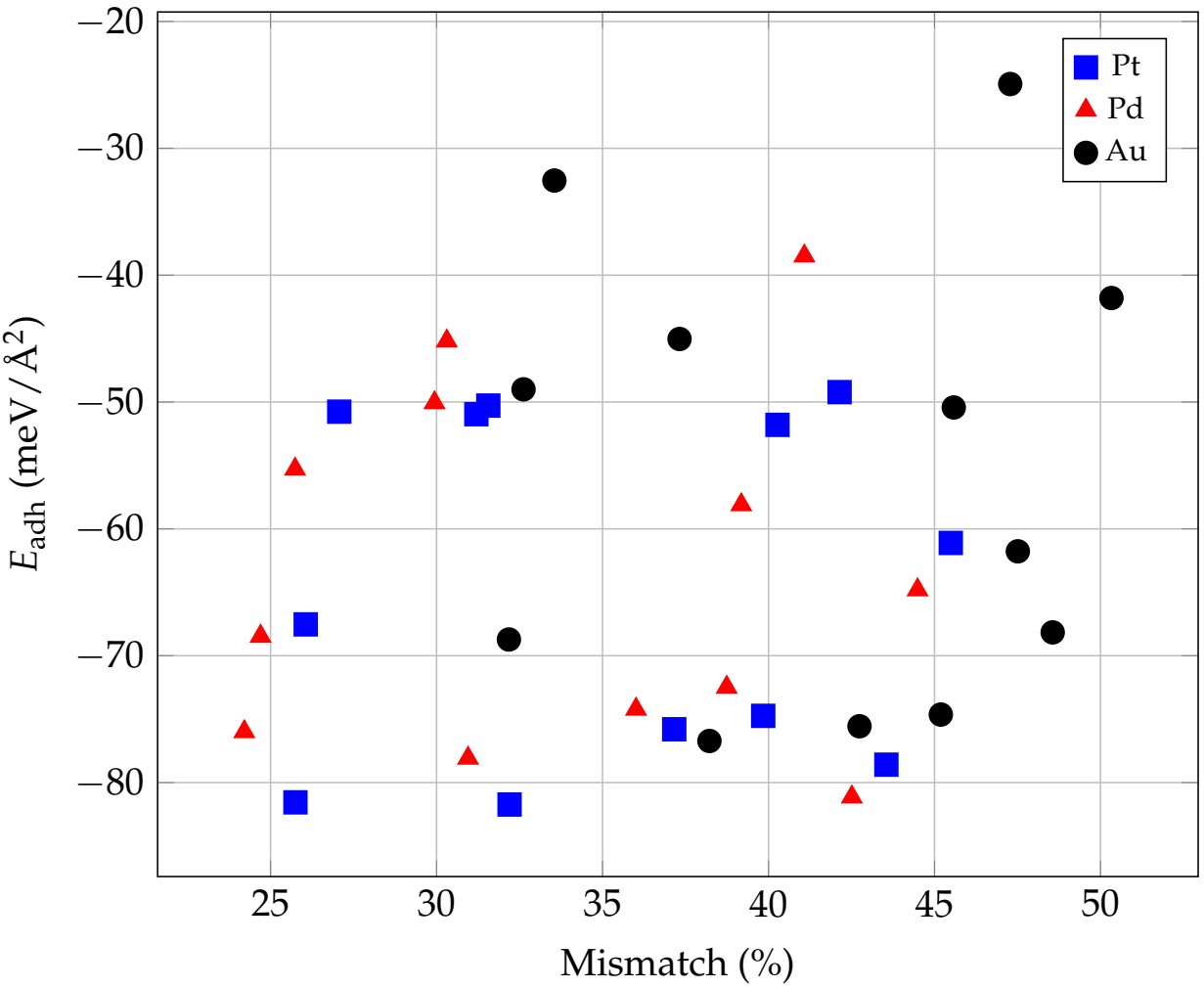

Figure S16: Plot of the adhesion energy (E_{adh}) as a function of the size mismatch for selected structures.

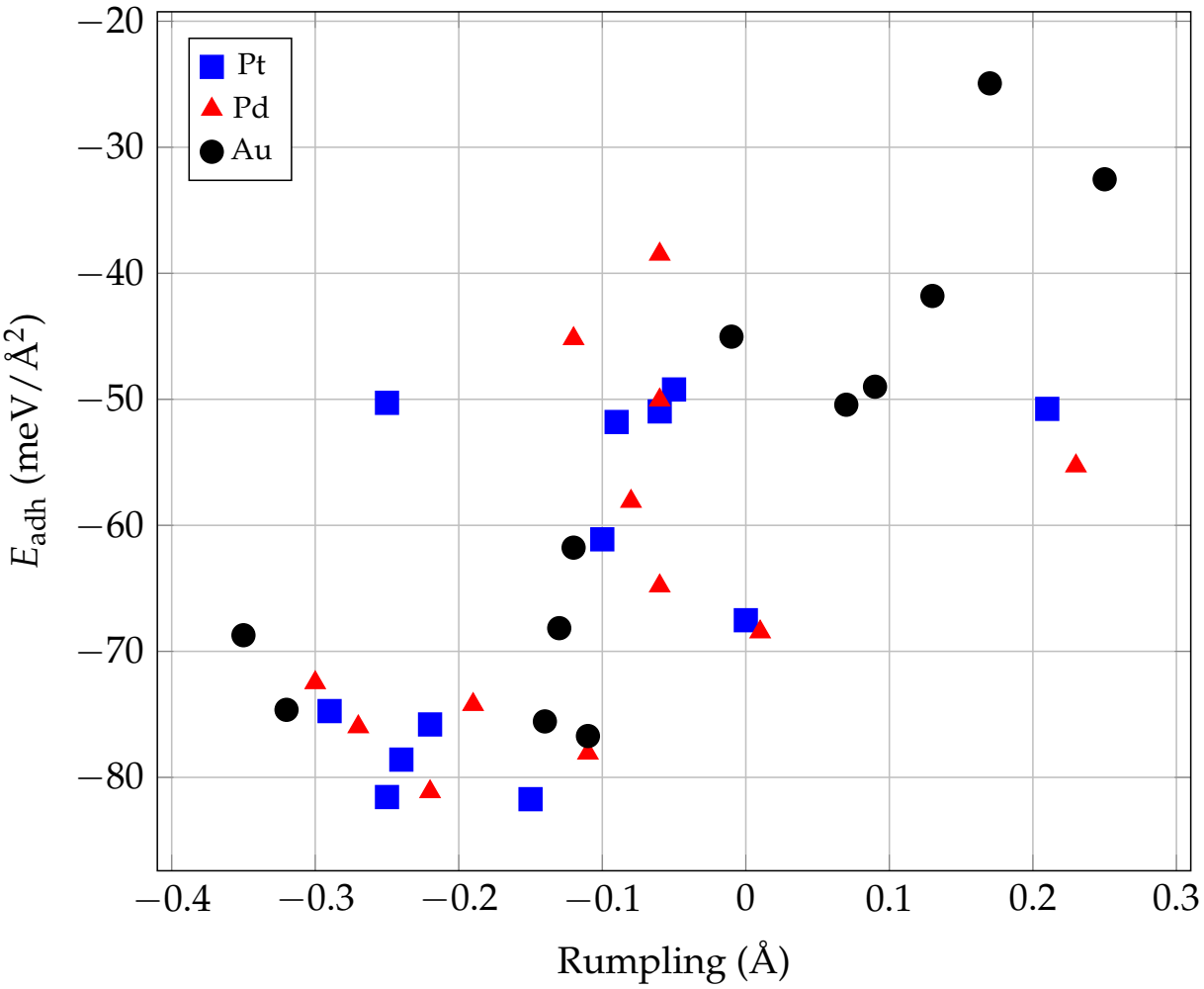

Figure S17: Plot of the adhesion energy (E_{adh}) as a function of the rumpling (R) for selected structures.

Electronic properties

Density of states

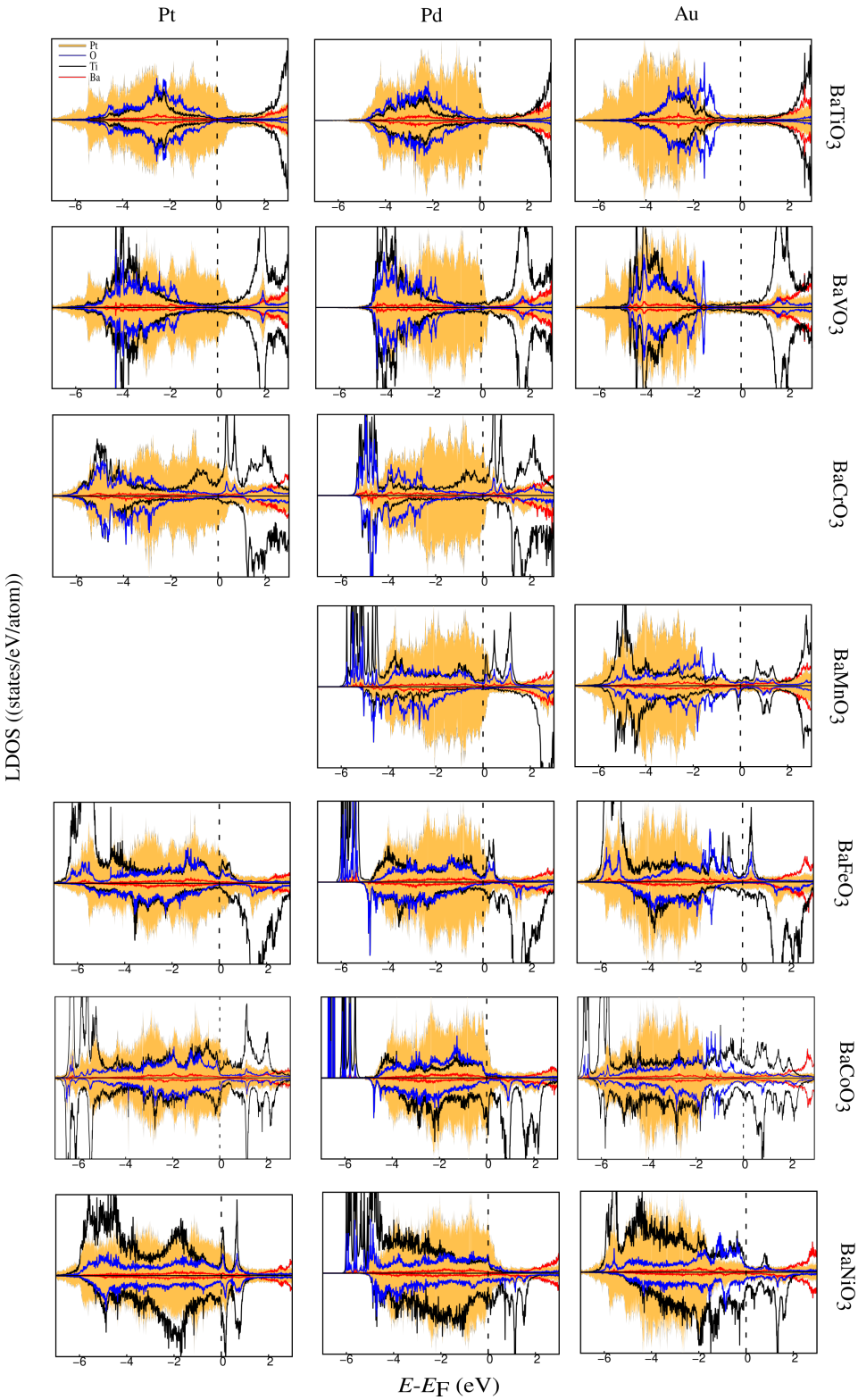

Figure S18: LDOS per atom for BaBO$_3$ (B = Ti, V, Cr, Mn, Fe, Co, Ni) with Pt, Pd, and Au substrates. Me, Ba, B, and O are represented by orange, red, black, and blue colors, respectivelly, as indicated in the top-left plot.

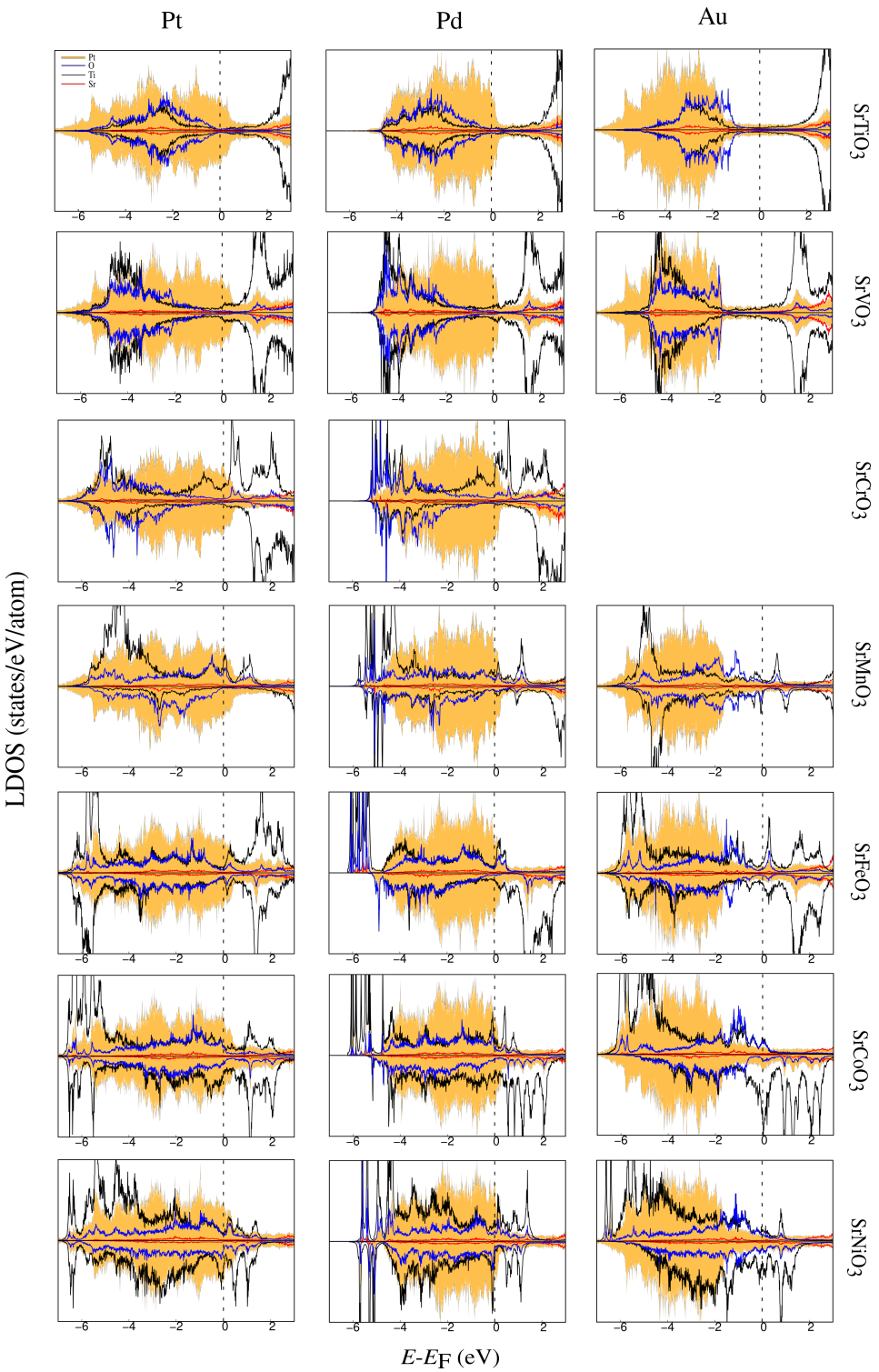

Figure S19: LDOS per atom for SrBO$_3$ (B = Ti, V, Cr, Mn, Fe, Co, Ni) with Pt, Pd, and Au substrates. Me, Sr, B, and O are represented by orange, red, black, and blue colors, respectivelly, as indicated in the top-left plot.

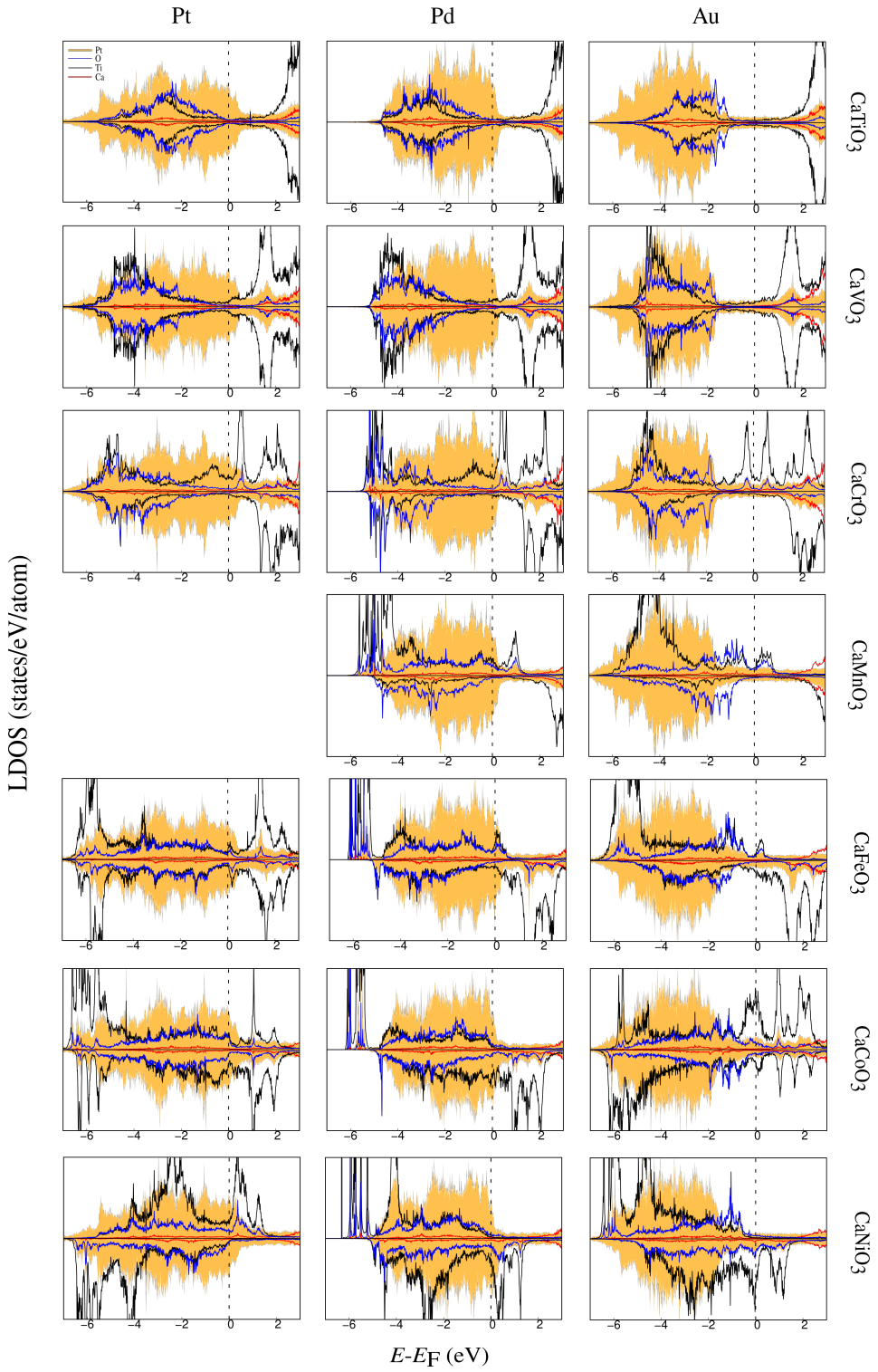

Figure S20: LDOS per atom for CaBO$_3$ (B = Ti, V, Cr, Mn, Fe, Co, Ni) with Pt, Pd, and Au substrates. Me, Ca, B, and O are represented by orange, red, black, and blue colors, respectivelly, as indicated in the top-left plot.

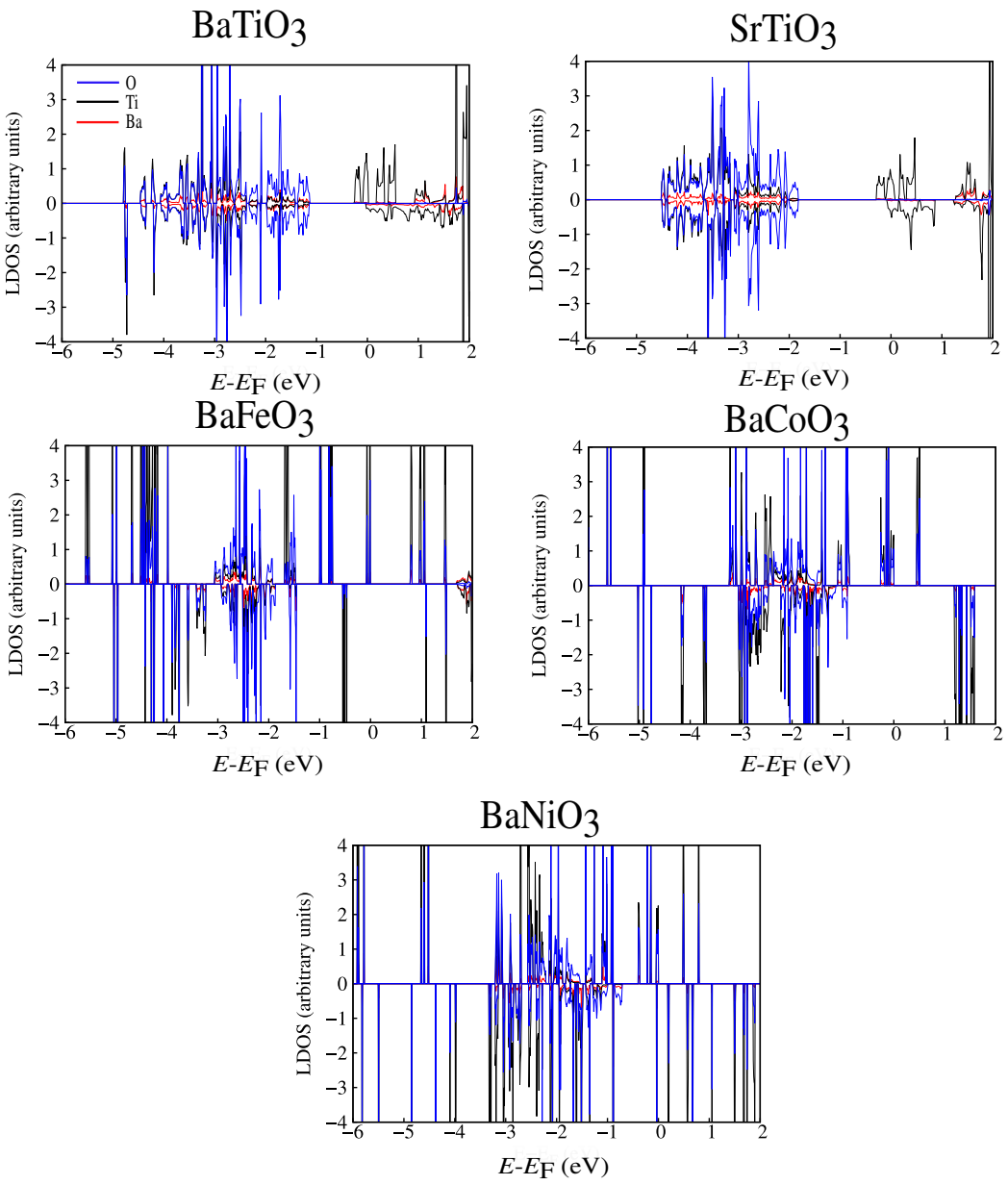

Figure S21: LDOS per atom for the oxide freestanding layers. Ba, B, and O are represented by red, black, and blue colors, respectivelly, as indicated in the top-left plot.

COHP and ICOHPs

(a) Ti–Pt

(b) Ti–Au

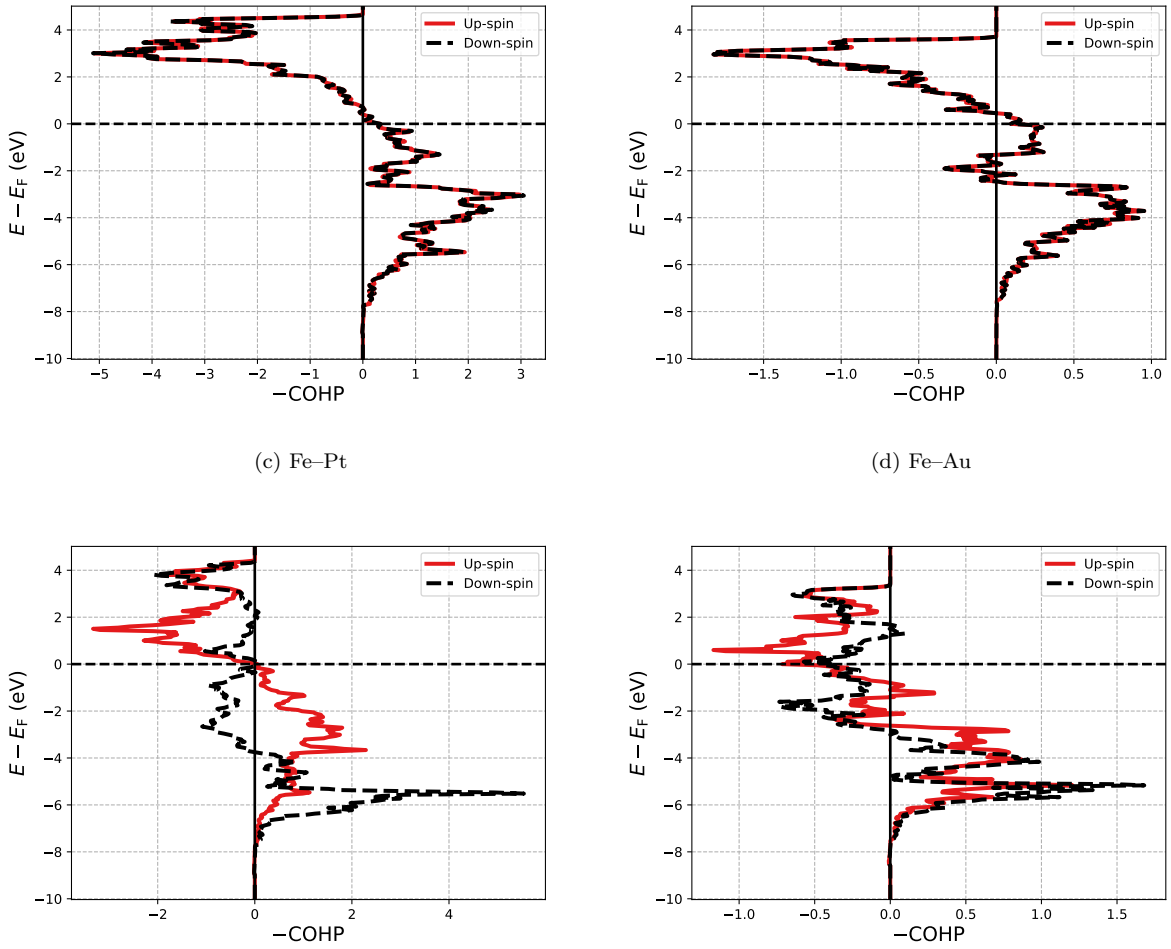

(c) Fe–Pt

(d) Fe–Au

Figure S22: COHPs between all bonds up to 3Å in the BaBO$_3$/Pt(111) systems (with B = Ti, Fe).

(a) Co–Pt

(b) Co–Au

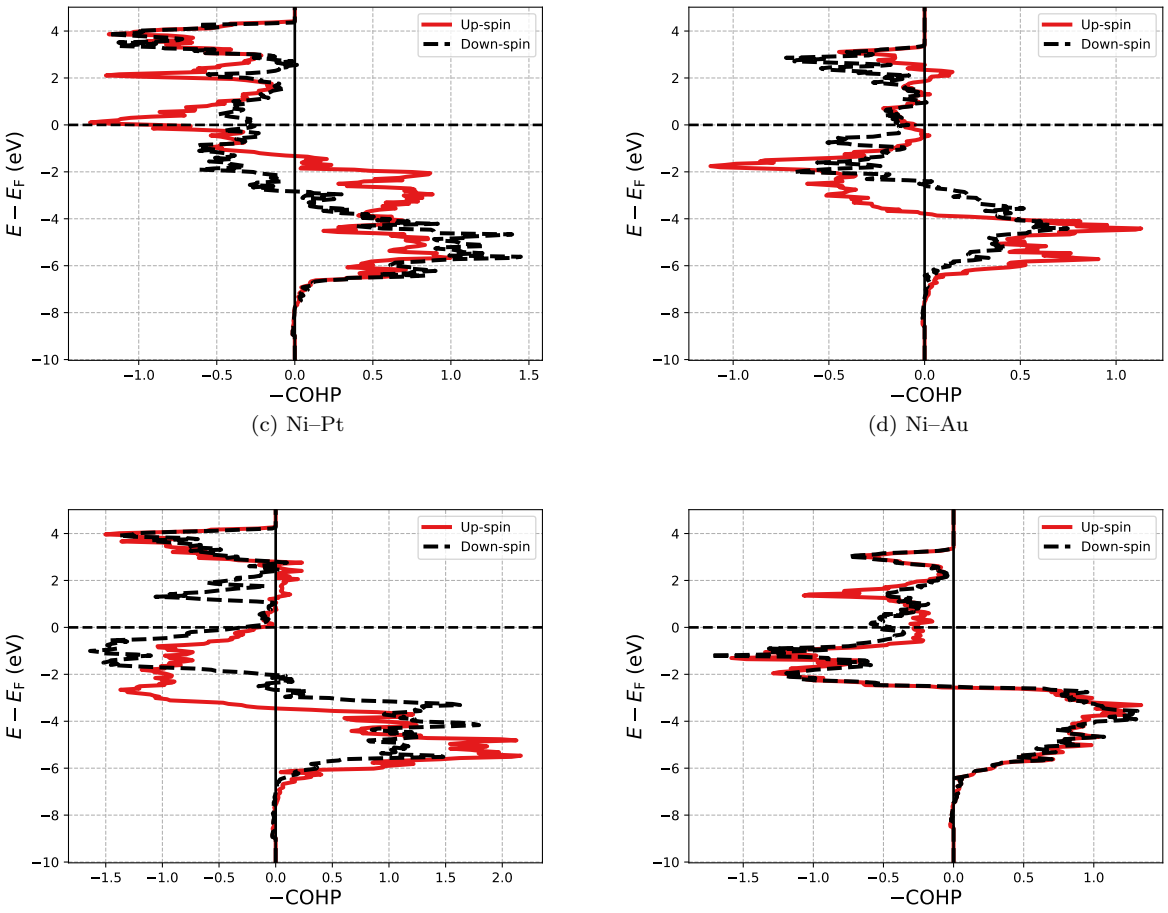

(c) Ni–Pt

(d) Ni–Au

Figure S23: COHPs between all bonds up to 3Å in the BaBO$_3$/Pt(111) systems (with B = Co, Ni).

(a) Ti–O (with Pt)

(b) Ti–O (with Au)

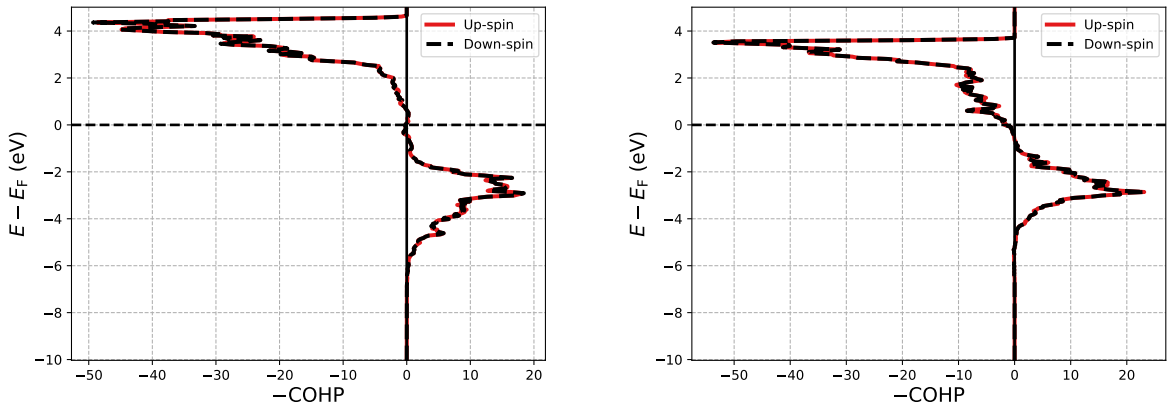

(c) Fe–O (with Pt)

(d) Fe–O (with Au)

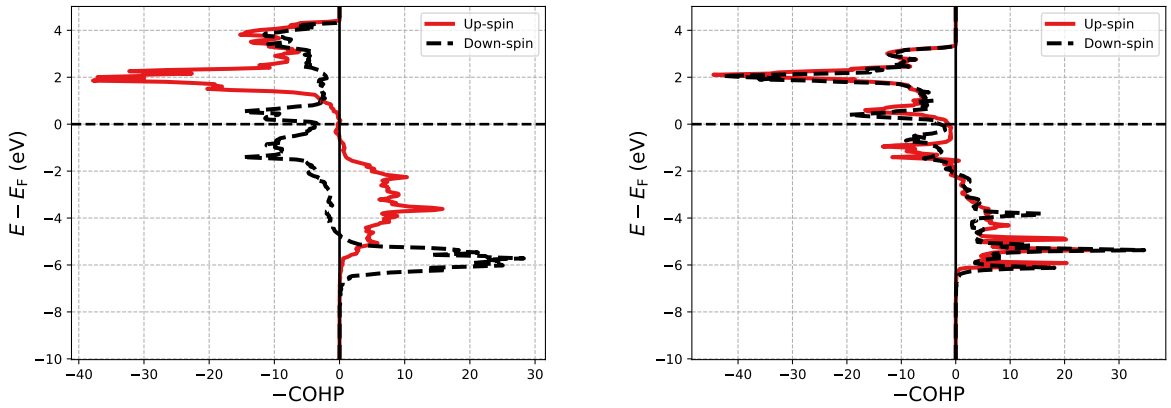

Figure S24: COHPs between all bonds up to 3Å in the BaBO$_3$/Me(111) systems (with B = Ti, Fe).

(a) Co–O (with Pt)

(b) Co–O (with Au)

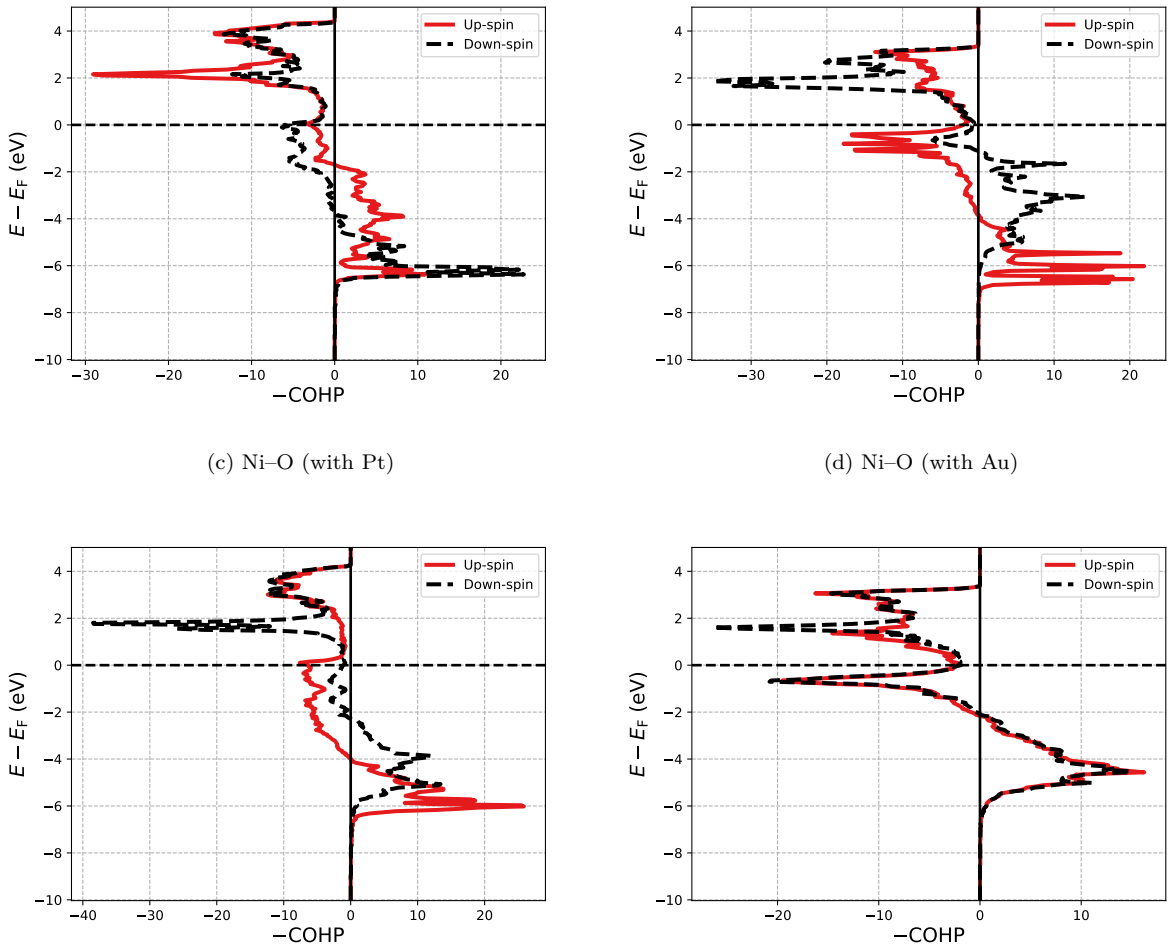

(c) Ni–O (with Pt)

(d) Ni–O (with Au)

Figure S25: COHPs between all bonds up to 3Å in the BaBO$_3$/Pt(111) systems (with B = Co, Ni).

(a) Pt–O (with Ti)

(b) Au–O (with Ti)

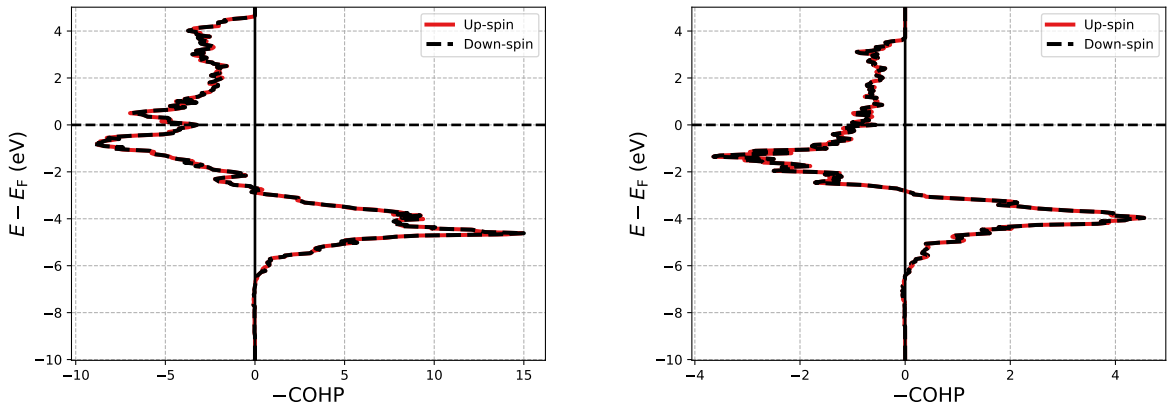

(c) Pt–O (with Fe)

(d) Au–O (with Fe)

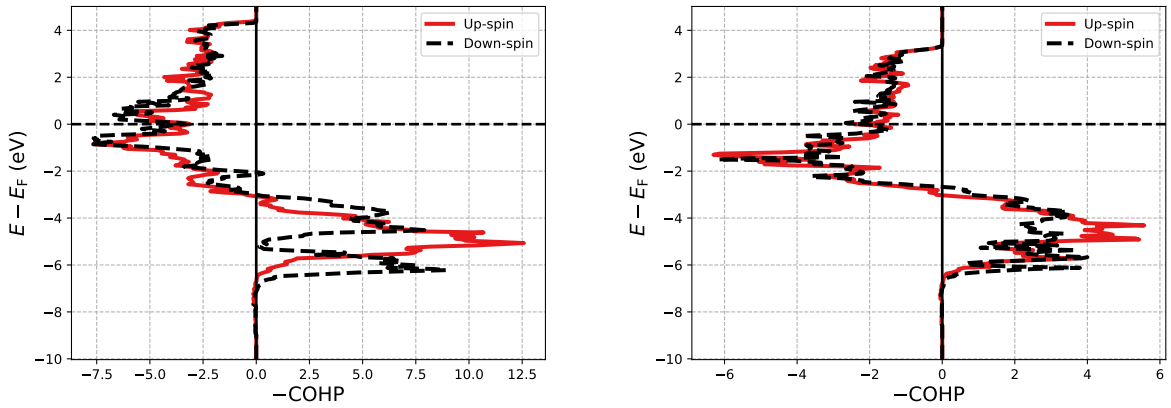

Figure S26: COHPs between all bonds up to 3Å in the BaBO$_3$/Me(111) systems (with B = Ti, Fe).

(a) Pt–O (with Co)

(b) Au–O (with Co)

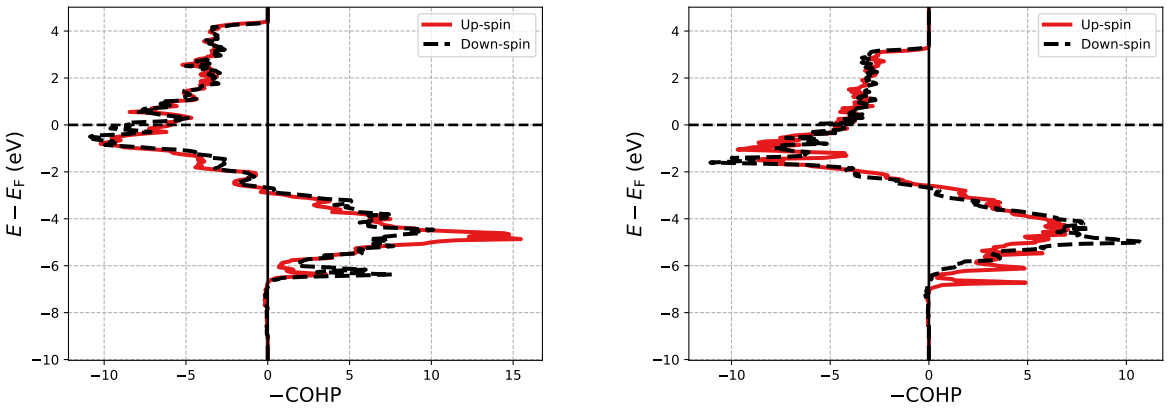

(c) Pt–O (with Ni)

(d) Au–O (with Ni)

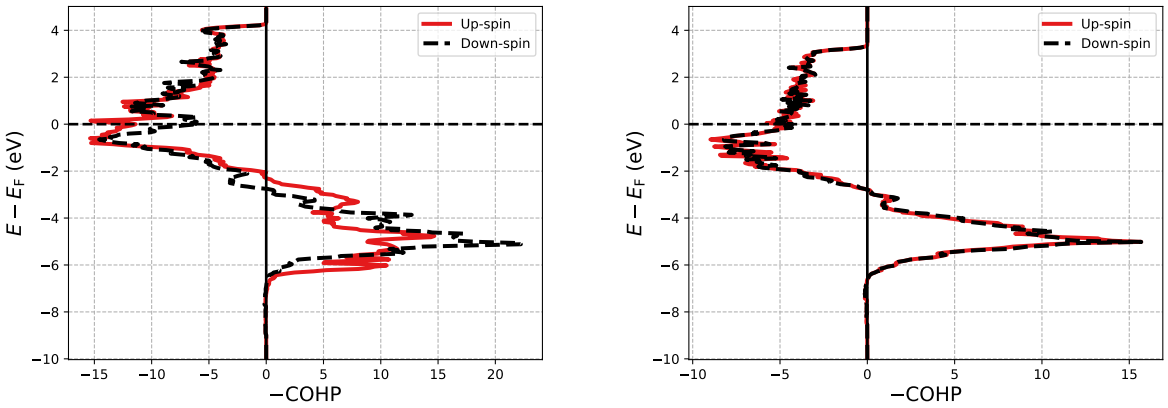

Figure S27: COHPs between all bonds up to 3Å in the BaBO$_3$/Pt(111) systems (with B = Co, Ni).

Elemental metals and bulk perovskites

Table S9: Lattice parameters, space groups, cohesive energies of the metals taken as references to calculate the formation enthalpies of OQAs and SHSs.

Metal	Structure	a (Å)	c (Å)	Cohesive energy (eV/at.)	Ref.
Ba	bcc ($Im\bar{3}m$)	4.99		−1.91	this work
		5.03		−1.88	PBE[1]
		5.01		−1.91	exp.[2,3]
Sr	fcc ($Fm\bar{3}m$)	6.02		−1.57	this work
		6.02		−1.62	PBE[1]
		6.08		−1.73	exp.[3,4]
Ti	hcp ($P6_3mmc$)	2.93	4.64	−5.17	this work
		2.95	4.68	−5.47	PBE[1,5]
		2.93	4.67	−5.45	PBE[6]
		2.95	4.68	−4.85	exp.[3,4]
V	bcc ($Im\bar{3}m$)	2.98		−5.45	this work
		3.00		−5.92	PBE[1]
		2.98		−6.03	PBE[6]
		3.03		−5.31	exp.[3,4]
Fe	bcc ($Im\bar{3}m$)	2.83		−4.97	this work
		2.83		−4.32	PBE[6]
		2.83		−4.85	PBE[1]
		2.86		−4.28	exp.[3,4]
Co	hcp ($P6_3mmc$)	2.50	4.02	−4.89	this work
		2.49	4.01	−4.44	PBE[6]
		2.50	4.09	−5.14	PBE[1]
		2.51	4.07	−4.39	exp.[3,7]
Ni	fcc ($Fm\bar{3}m$)	3.53		−4.75	this work
		3.52		−4.48	PBE[6]
		3.52		−4.83	PBE[1]
		3.92		−4.44	exp.[3,4]
Pt	fcc ($Fm\bar{3}m$)	3.99		−5.63	this work
		3.95		−5.87	PBE[6]
		3.98		−5.32	PBE[1]
		3.92		−5.84	exp.[3,4]
Au	fcc ($Fm\bar{3}m$)	4.18		−3.18	this work
		4.17		−3.83	PBE[6]
		4.16		−3.11	PBE[1]
		4.07		−3.81	exp.[3,4]

Table S10: Lattice parameters, space groups and formation enthalpies of perovskites considered in the thermodynamic model.

Perovskite	Structure	a (Å)	b (Å)	c (Å)	Formation enthalpy (eV/at.)	Ref.
$BaTiO_3$	$Pm\bar{3}m$	4.05			−3.35	this work
	$R3m$	4.08 (α=89.67°)			−3.50	PBE[8]
$SrTiO_3$	$Pm\bar{3}m$	3.96			−3.38	this work
	$Pm\bar{3}m$	3.94			−3.56	PBE[8]
$BaFeO_3$	$Pm\bar{3}m$	4.01			−2.07	this work
	$Pm\bar{3}m$	4.03			−2.25	PBE[8]
$BaCoO_3$	$Cmcm$	5.70	9.99	4.81	−1.83	this work
	$P6_3mmc$	5.74		5.77	−2.11	PBE[8]
$BaNiO_3$	$P6_3mmc$	5.71		4.80	−1.48	this work
	$P6_3mmc$	5.72		4.83	−1.48	PBE[8]

Magnetic stability

Table S11: Magnetic stability considering, as the initial magnetic moment, a ferromagnetic (FM) and an antiferromagnetic (AFM) state of the B (B = Cr, Mn, Fe, Co, Ni) elements in the approximant structure. Since there are four B atoms in the approximant with two equivalent positions, we consider the initial AFM state with the m_B of the non-equivalent positions in opposite directions. RMS = Resulting magnetic moment; IMC = Initial magnetic configuration; SIC = Stable as initial configuration.

Formula	Energy FM (eV/at.)	Energy AFM (eV/at.)	RMC (IMC = FM)	RMS (IMC = AFM)	$\overline{m}_B$ (μ_B) (IMS = FM)	$\overline{m}_B$ (μ_B) (IMS = AFM)	SIC
$Pt_{120}Ba_5Cr_4O_{12}$	−3.15717	−3.15781	FM	AFM	1.09	−0.03	AFM
$Pt_{120}Ba_5Fe_4O_{12}$	−3.09922	−3.09826	FM	AFM	3.32	−0.12	FM
$Pt_{120}Ba_5Co_4O_{12}$	−3.02495	−3.02418	AFM	FM	0.04	−2.69	FM
$Pt_{120}Ba_5Ni_4O_{12}$	−2.98047	−2.96809	FM	AFM	0.59	−0.67	FM
$Pt_{120}Sr_5Cr_4O_{12}$	−3.13384	−3.13454	FM	FM	1.16	1.17	AFM
$Pt_{120}Sr_5Fe_4O_{12}$	−3.07669	−3.07763	AFM	AFM	−0.12	−0.14	AFM
$Pt_{120}Sr_5Co_4O_{12}$	−2.99597	−2.99534	AFM	AFM	−0.04	−0.04	FM
$Pt_{120}Sr_5Ni_4O_{12}$	−2.9303	−2.95691	AFM	AFM	0.69	0.32	AFM
$Pt_{120}Ca_5Fe_4O_{12}$	−3.08253	−3.08354	AFM	AFM	−0.26	−0.2	AFM
$Pt_{120}Ca_5Co_4O_{12}$	−3.0078	−3.00612	AFM	AFM	−0.11	−0.11	FM
$Pt_{120}Ca_5Ni_4O_{12}$	−2.95689	−2.9563	AFM	FM	0.03	1.44	FM
$Pd_{120}Ba_5Cr_4O_{12}$	−2.08172	/	AFM	/	0.59	/	FM
$Pd_{120}Ba_5Mn_4O_{12}$	−2.01345	/	AFM	/	0.92	/	FM
$Pd_{120}Ba_5Fe_4O_{12}$	−2.02899	−2.03089	FM	FM	3.58	3.58	AFM
$Pd_{120}Ba_5Co_4O_{12}$	−1.95797	−1.95604	FM	FM	2.57	−2.57	FM
$Pd_{120}Ba_5Ni_4O_{12}$	−1.89289	−1.9067	FM	AFM	1.49	−0.03	AFM
$Pd_{120}Sr_5Cr_4O_{12}$	−2.05863	−2.05942	FM	FM	1.21	1.23	AFM
$Pd_{120}Sr_5Fe_4O_{12}$	−2.01027	−2.01489	FM	FM	3.47	3.76	AFM
$Pd_{120}Sr_5Co_4O_{12}$	−1.94105	/	FM	/	2.59	/	FM
$Pd_{120}Sr_5Ni_4O_{12}$	−1.88425	−1.88285	FM	AFM	−0.48	0.4	FM
$Pd_{120}Ca_5Cr_4O_{12}$	−2.072	/	FM	/	1.14	/	FM
$Pd_{120}Ca_5Fe_4O_{12}$	−2.01331	−2.01448	FM	AFM	3.5	0.26	AFM
$Pd_{120}Ca_5Co_4O_{12}$	−1.93052	−1.93402	AFM	AFM	1.04	0.12	AFM
$Pd_{120}Ca_5Ni_4O_{12}$	−1.89952	−1.89853	AFM	FM	0.7	1.45	FM
$Au_{120}Ba_5Mn_4O_{12}$	−0.72306	/	AFM	/	1.77	/	FM
$Au_{120}Ba_5Fe_4O_{12}$	−0.72789	−0.73004	AFM	FM	−0.0	3.4	AFM
$Au_{120}Ba_5Co_4O_{12}$	−0.6368	−0.6345	FM	FM	−2.77	2.76	FM
$Au_{120}Ba_5Ni_4O_{12}$	−0.56556	−0.57633	FM	AFM	1.17	−0.05	AFM
$Au_{120}Sr_5Fe_4O_{12}$	−0.69417	−0.69365	AFM	AFM	1.5	−0.03	FM
$Au_{120}Sr_5Co_4O_{12}$	−0.61276	−0.61436	FM	AFM	−2.41	−0.11	AFM
$Au_{120}Sr_5Ni_4O_{12}$	−0.56751	−0.56264	FM	AFM	0.44	−0.01	FM
$Au_{120}Ca_5Cr_4O_{12}$	−0.75502	/	AFM	/	0.65	/	FM
$Au_{120}Ca_5Fe_4O_{12}$	−0.70948	−0.70957	FM	AFM	3.65	0.17	AFM
$Au_{120}Ca_5Co_4O_{12}$	−0.61741	−0.61429	AFM	FM	−1.33	2.66	FM
$Au_{120}Ca_5Ni_4O_{12}$	−0.56905	/	FM	/	1.24	/	FM

References

(1) Lejaeghere, K.; Speybroeck, V. V.; Oost, G. V.; Cottenier, S. Error estimates for solid-state density-functional theory predictions: an overview by means of the ground-state elemental crystals. *Critical Reviews in Solid State and Materials Sciences* **2014**, *39*, 1–24.

(2) Barrett, C. S. The crystal structure of barium and europium at 293, 78 and 5 K. *Journal of Chemical Physics* **1956**, *25*, 1123–1124.

(3) Kittel, C. *Introduction to Solid State Physics*, 7th ed.; John Wiley & Sons: USA, 1996.

(4) Villars, P.; Calvert, L. D. *Pearson´s Handbook of Crystallographic Data for Intermetallic Phases*; ASM International: Metals Park, Ohio, USA, 1998.

(5) Spreadborough, J.; Christian, J. The measurement of the lattice expansions and Debye temperatures of titanium and silver by X-ray methods. *Proceedings of the Physical Society (1958-1967)* **1959**, *74*, 609.

(6) Janthon, P.; Luo, S.; Kozlov, S. M.; Vines, F.; Limtrakul, J.; Truhlar, D. G.; Illas, F. Bulk Properties of Transition Metals: A Challenge for the Design of Universal Density Functionals. *J. Chem. Theory Comput.* **2014**, *10*, 3832–3839.

(7) Hofer, L. J. E.; Peebles, W. C. Preparation and X-Ray Diffraction Studies of A New Cobalt Carbide. *J. Am. Chem. Soc.* **1947**, *69*, 893–899.

(8) Jain, A.; Hautier, S. P. O. G.; Chen, W.; Richards, W. D.; Dacek, W.; Cholia, S.; Gunter, D.; Skinner, D.; Ceder, G.; Persson, K. A. Commentary: The Materials Project: A materials genome approach to accelerating materials innovation. *APL Mater.* **2013**, *1*, 011002.

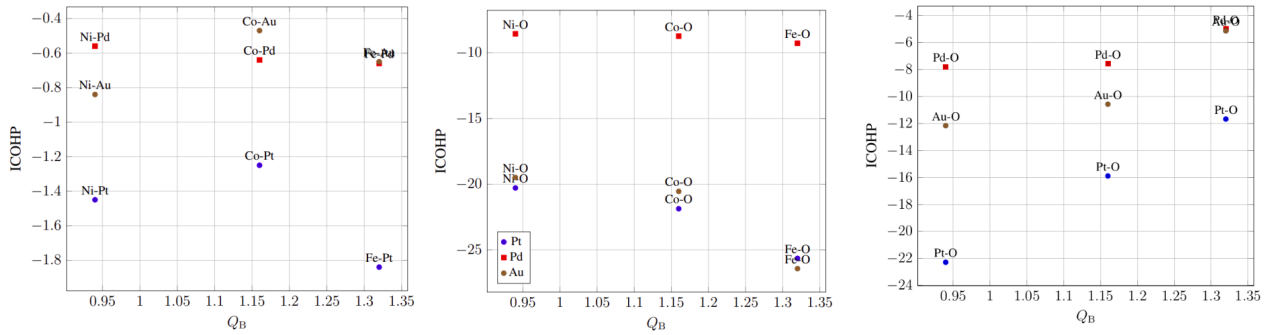

(a) (b) (c)

Fig. S30 : ICOHP (eV) as a function of the Bader charge on the transition metal (Q_B) : TM-substrate bonds (a), TM-O bonds (b) and substrate-O bonds (c)